Investigation of the Magnetoresistance Quantum Oscillations in Magnesium*

Frank E. Richards[†]

The Department of Physics and the James Franck Institute, The University of Chicago, Chicago, Illinois 60637
(Received 30 August 1972)

The magnetoresistance (MR) oscillations in Mg have been systematically investigated. The small-amplitude MR oscillations have been recorded simultaneously with the de Haas–van Alphen (dHvA) oscillations as a function of magnetic field, field orientation, and temperature. Several new experimental problems peculiar to small-amplitude MR oscillation work in metals are discussed in detail. A theoretical analysis of the experimental deviations from the predictions of current Shubnikov–de Haas (SdH) theory is given. It is found that when magnetic breakdown causes deviation from the normal MR field dependence, it also causes deviation from the present SdH theory. Five basic mechanisms for MR oscillation are discussed, the SdH and four non-SdH mechanisms. Because magnesium is already well understood, and because the dHvA oscillations provided a reliable basis for interpretation of the data, the MR oscillations could be sorted out and classified in terms of the basic mechanisms.

I. INTRODUCTION

Of the various magnetic-field-dependent quantum-oscillation effects which yield Fermi-surface information, the most studied are the de Haas-van Alphen (dHvA) effect in metals and semimetals and the Shubnikov-de Haas (SdH) effect in semimetals and degenerate semiconductors. The reason for this is that one normally chooses to measure the largest amplitude effect in the given material. The SdH oscillations in metals have not been studied in detail to date because of their small amplitudes and resultant difficulty of observation. The present paper reports a systematic study in high-purity magnesium of the small-amplitude magnetoresistance (MR) oscillations due to the SdH and other quantum-oscillation mechanisms.

Historically, MR oscillations in metals were assumed to be SdH oscillations so that comparison with the theoretical field dependence led to grave doubts about the theory. It was then discovered that magnetic breakdown (MB) could cause large-amplitude MR oscillations, and since then the tendency has been to assume that all readily observable MR oscillations in metals are due to this MB-oscillation mechanism. In addition to these two mechanisms, three other MR-oscillation mechanisms will be discussed in this paper. There are no *obvious* differences by which the various oscillation types might readily be distinguished, so that their identification requires careful deductive work.

In contrast, experimental dHvA signals are *not* complicated by any other oscillation mechanisms, even in a metal with a complicated Fermi surface and MB effects. The close relationship between the dHvA and SdH effects (which is explicitly expressed in Sec. II of this paper) can provide an extremely sensitive test of the theory of the SdH oscillations. In effect, the MR-oscillation amplitudes are normalized by dividing by the dHvA amplitudes, improving by orders of magnitude the sensitivity with which the field dependence of the observed MR-oscillation amplitude may be compared with the dependence predicted by the SdH theory. At the same time, the simultaneous recording of the dHvA amplitude also represents a very useful tool for the task of identifying the various types of MR oscillation. Since it is already well understood, the dHvA effect affords a reliable and firm basis from which to start in interpreting the observed MR oscillations.

The aim in this experiment was to separate, classify, and understand the origin of the various types of small-amplitude MR oscillations in magnesium, with the broader goal of testing the theory of the SdH effect. The dHvA- and MR-oscillation amplitudes were recorded simultaneously as a function of field and temperature, making possible a valid comparison of the two amplitudes. To the author's knowledge this has not been done before in any material. A preliminary version of this work has already been reported.[1]

Before introduction of the particular frequencies observed in this small-amplitude-oscillation experiment, it is appropriate to briefly discuss two *large-amplitude* MR-oscillation mechanisms. Both involve MB, and both have been studied in Mg already. First, the MB-oscillation mechanism mentioned above causes the MR oscillations usually reported in metals. For the magnetic field $\vec{H}$ along the [0001] crystallographic axis in Mg and Zn, this mechanism has been quantitatively treated by Falicov, Pippard, and Sievert,[2] and it has been reviewed for metals in general by Stark and Falicov.[3] The mechanism arises from the fact that MB affects the material's MR, sometimes controlling it. In some materials, the MR field dependence is completely changed by MB, either from quadratic to saturated or from saturated to quadratic field dependence, i.e., from one behavior category to

the other. In Mg, the key MB process is the destruction of exact carrier compensation for $\vec{H}$ along [0001], the $\hat{c}$ axis, or the creation of open orbits along the $\hat{c}$ axis for $\vec{H}$ lying in the basal plane. As the density of states oscillates, periodic in H^{-1}, the probability of the key MB process occurring must therefore oscillate too, at frequencies corresponding to all those extremal orbits taking part in the key MB process. The MR then *tends* to oscillate between its old behavior curve and its new final curve, giving rise to *large* MR oscillations. The second large-amplitude MR-oscillation mechanism is the "path-interference" oscillation discovered recently by Stark and Friedberg in Mg,[4] and subsequently found[5] and analyzed[6] in Sn. The origin of this oscillation is the self-interference of the electron wave after traversing two (or more) different paths, an already familiar concept from basic quantum theory. This oscillation arises only on MB-coupled networks or MB open orbits, and therefore exists in Mg only for the same field orientations as for the first oscillation mechanism. Both of these large-amplitude oscillation mechanisms were avoided in this investigation of small-amplitude MR oscillations, by staying at least 2° away from the above orientations.

Magnesium was selected primarily because it met the requirement of having been thoroughly studied, its Fermi surface reliably and accurately known.[7-10] In particular, magnetic breakdown in Mg is well enough understood that we could choose a few extremal orbits which reliably do not involve MB and a few which do involve MB. Figure 1 shows Mg's spectrum of dHvA frequencies,[8] corresponding to the extremal orbits on its Fermi surface. Its spectrum reflects the complexity of its Fermi surface. In this experiment the oscillation amplitudes from the six orbits indicated in Fig. 1 were measured at the three field orientations $\theta = 40°$, $\theta = 70°$, and $\theta = 88°$. The latter orientation is 2° away from the basal plane orientation [11$\bar{2}$0], at which open orbits exist. The three orbits not involving MB were μ_1^5 (88°) (the monster waist), μ_1^5 (70°), and λ_1^1 (88°) (the lens). The other three orbits, containing MB junctions, were C_1^1 (88°) (the clam), γ_1^1 (40°) (the cigar), and μ_1^6 (40°) (the monster intersection). The MB orbit C_1^1 does not exist on the $H = 0$ Fermi surface—it is a MB-coupled orbit arising only after MB begins. In contrast, the (MB) orbits γ_1^1 (40°) and μ_1^6 (40°) do exist on the $H = 0$ Fermi surface; when coupled by MB, they give rise to the MB-coupled orbit D_1^1 in Fig. 1. Concerning the nature of these six MR oscillations, it may be stated with certainty that none of the six orbits takes part in an open orbit or in destruction of exact carrier compensation.[8,9] Therefore, the two large-amplitude oscillation

mechanisms discussed above cannot contribute to the measured amplitudes.

The availability of Mg of high purity was an additional reason for its selection. In this experiment, the quantum oscillations were damped by scattering less seriously than in most dHvA work in other pure metals.

Data were recorded as a function of H (to 36 kG) at $T = 1.37$ K and as a function of T (down to 1.37 K) at a high-field value appropriate for each orbit. Only the fundamental or principal harmonic amplitude was measured.

The other pertinent ranges and conditions were as follows: The quantum number $n(\nu)$ of the Landau level at the ν extremal orbit always satisfied the condition $n \gg 1$, with values from about 1340 to 135. All work was done in the asymptotic region of the magnetoresistivity $\omega\tau \gg 1$, where $\omega\tau$ is an effective value characteristic of the whole Fermi surface, ω is the cyclotron frequency $\omega_c = eH/m^*c$, and τ is the relaxation time appearing in the magnetoresistivity tensor element ρ^{ij}. On the basis of the simple equation

$$\rho^{yy}(H) = \rho^{yy}(0)[1 + (\omega\tau)^2],$$

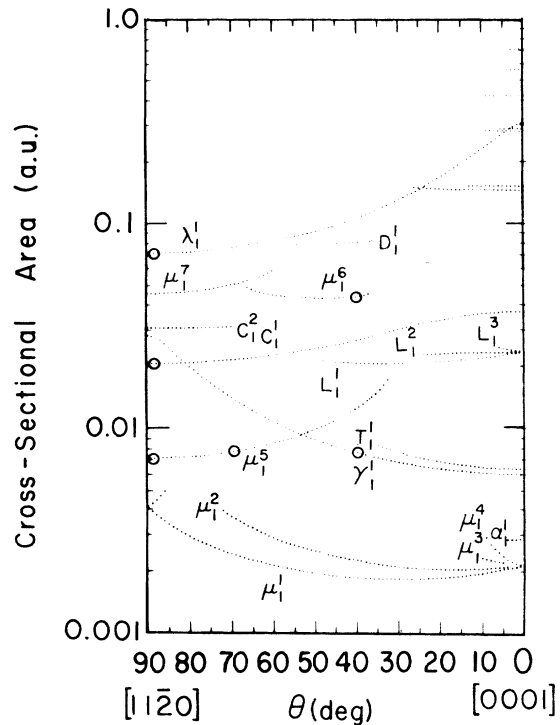the value of $\omega\tau$ was estimated to range from 310 to

FIG. 1. dHvA spectrum of extremal areas in Mg (Ref. 8) as a function of θ, the field orientation. The six cases investigated in the present paper are identified by circles. The cross-sectional area α_i (a.u.) is related to the observed oscillation frequency F_i (G) by the relationship α_i (a.u.) $= 2.673 \times 10^{-9} F_i$ (G).

1600 for the field values of this experiment. The final consideration is the assumption, made in Sec. II, that only the sample's bulk was important as a source of the signals, i.e., that the surface region may be neglected. This condition will be discussed elsewhere in the present paper.

The remaining sections of this paper are as follows: Sec. II, SdH theory; Sec. III, experimental procedure; Sec. IV, results and discussion; and Sec. V, summary.

II. SdH THEORY

The presentation and analysis of the data, using the well-understood dHvA amplitudes to make possible a reliable comparison of the MR-oscillation amplitudes with predictions of the SdH theory, revealed that the SdH literature did not contain a suitable framework within which to present these data. The development of such a framework involves two principal problems, the solutions to which are presented in the present section. First, without relying on the approximations usually made, such as $\rho^{xx} = 1/\sigma^{xx}$, one would like to avoid measuring *all* of the tensor elements ρ^{ij} (including its nonoscillatory part ρ_0^{ij} and its oscillatory part $\Delta\rho^{ij}$) in order to invert the full tensor ρ^{ij} for comparison with the theoretical tensor σ^{ij}. This goal is accomplished by deriving an exact relationship between the ratio $\Delta\rho^{ij}/\rho_0^{ij}$ and the corresponding magnetoconductivity ratio $\Delta\sigma^{ij}/\sigma_0^{ij}$, which is valid under the same conditions under which the SdH theory itself is valid, for the class of materials to which Mg belongs. Second, the relationship between the dHvA and SdH oscillations has not previously been explicitly expressed in the literature, for general experimental conditions. Also, the precise relationship between the parameters measured via the two effects has not previously been rigorously considered. With these preliminary problems solved, an appropriate framework is then found within which to present and analyze the MR-oscillation data. Only the SdH mechanism of MR oscillations is considered.

The SdH oscillations $\Delta_\nu\sigma^{ij}$ of the magnetoconductivity tensor element σ^{ij} arise from oscillations in the Fermi-surface density of states $\mathfrak{N}$,

$$\mathfrak{N} = \mathfrak{N}_0 + \sum_\nu \Delta_\nu\mathfrak{N}, \tag{1}$$

where $\mathfrak{N}_0$ is the nonoscillatory or average background and $\Delta_\nu\mathfrak{N}$ is the oscillation due to the νth extremal orbit.[11] Analogous notation will be used for σ^{ij} and ρ^{ij}, e.g.,

$$\sigma^{ij} = \sigma_0^{ij} + \sum_\nu \Delta_\nu\sigma^{ij} .$$

The density-of-states oscillation $\Delta_\nu\mathfrak{N}$ gives rise to $\Delta_\nu\sigma^{ij}$ both directly through the density of states and indirectly through scattering from any point

on the Fermi surface into $\Delta_\nu\mathfrak{N}$. The probability of scattering is proportional to the available density of states and therefore oscillates, which in turn causes oscillations of the magnetoconductivity.

The theory of Adams and Holstein (1959)[12] is based on a quantum calculation of the SdH effect for a spherical Fermi surface (FS) with arbitrary but fixed effective mass and for isotropic elastic scattering. Their treatment of intralevel scattering at ν on the Fermi surface (which means scattering between degenerate quasiparticle states in the Landau level) has been corrected in the more recent quantum calculation by Kubo, Miyaki, and Hashitsume (1965).[13] The results of the latter are given in the Appendix—as restated by Roth and Argyres (1966)[14] to include the spin splitting factor S_r. When the terms from intralevel scattering are omitted (see next paragraph), these current theories all give the following result:

$$\frac{\Delta_\nu\sigma^{ij}}{\sigma_0^{ij}} = B_\nu^{ij} \frac{\Delta_\nu\mathfrak{N}'}{\mathfrak{N}_0} , \tag{2a}$$

where

$$\Delta_\nu\mathfrak{N}' = A\sqrt{H}\, 2\sum_{r=1}^{\infty} \frac{e_r}{\sqrt{r}}\cos\left[2\pi r\left(\frac{F}{H} - \gamma\right) \mp \frac{\pi}{4}\right]. \tag{2b}$$

In Eqs. (2), B_ν^{ij} is a constant, independent of H and T—specifically, $B_\nu^{xx} = B_\nu^{yy} = +\frac{5}{2}$, $B_\nu^{xy} = 0$, and $B_\nu^{zz} = -1$ for the model FS mentioned above. In Eq. (2b), the oscillation takes place as a function of $1/H$ with a frequency F and phase factor γ, and it is a summation over harmonics beginning with the fundamental. Besides $H^{1/2}$, the only amplitude factors which depend on H and T are the Landau-level-width damping factor K_r and the temperature broadening factor I_r contained in the total damping factor e_r,[11]

$$e_r = I_r K_r S_r .$$

The expressions for these factors are well known: $I_r = rX/\sinh rX$, where $X = 2\pi^2 kT/\hbar\omega$, $\omega = eH/m^*c$, and m^* is the effective mass; and $K_r = e^{-rX_D}$, where X_D may be written either as $2\pi^2 kT_D/\hbar\omega$ or $\pi/\omega\tau_\Gamma$. Here T_D is the Dingle temperature and τ_Γ is the lifetime or τ_Γ^{-1} is the relaxation rate of the quasiparticle states in the Landau level, and they are equivalent measures of the Landau-level half-width Γ, since

$$\tau_\Gamma^{-1} = 2\pi\hbar^{-1}kT_D \tag{3}$$

holds. Finally, $A = (2m^*/\hbar^2)(e/c\hbar)^{1/2}(2\pi/|\alpha''|)^{1/2}$, where α is the extremal area in k space and α'' is its second derivative with respect to k_z, the component of $\vec{k}$ along $\hat{H} = \hat{z}$. For the above model FS, α'' is just 2π. The quantity $\Delta_\nu\mathfrak{N}'$ might be called "the temperature-broadened density-of-states oscillation," since it differs from $\Delta_\nu\mathfrak{N}$ only by the presence of I_r in e_r in (2b). (See Ref. 11.) The

coefficients B_ν^{ij} in Eqs. (2) may take the values appropriate for any given FS rather than the values given for the spherical model FS. Equations (2) with unrestricted B_ν^{ij} thus represent a common statement of the currently accepted SdH theories in a simple generalized form suitable for extension to materials with arbitrary Fermi surfaces. Indeed, Pippard arrives at general results which are of this form by what he calls an elementary treatment of the SdH effect for arbitrary Fermi surfaces.[15]

The effect of the intralevel scattering terms, which were omitted above, is to enhance both the nonoscillatory part σ_0^{ii} and the oscillatory part $\Delta_\nu\sigma^{ii}$ of the transverse elements σ^{ii} ($i = x$ or y), especially in the quantum limit when $n \to 1$. For isotropic elastic scattering these enhancements become important only when intralevel scattering becomes an appreciable fraction of the total scattering in or out of the Landau level at the extremal orbit; such behavior occurs only at lower quantum numbers. In the Appendix we have calculated these enhancements for the conditions of this experiment and isotropic elastic scattering. The calculated enhancements are a maximum of about 0.55% for σ_0^{ii} and $\leq 1\%$ for the six observed fundamental oscillations $\Delta_\nu\sigma^{ii}$ and hence need not be included in the present treatment.

It seems worthwhile to question, at this point, whether the currently accepted SdH theories offer an adequate basis for interpreting SdH MR oscillations in those actual materials which show unexplained MR behavior. In considering various possible causes for observed deviations from "normal" MR behavior (e.g., $\rho_0^{xx} \propto H^{2.00}$ in the asymptotic field region), we noticed that the SdH theory does not include any mechanism capable of causing a deviation from "normal" MR behavior, with the exception of intralevel scattering terms. Therefore, if the observed MR shows any unexplained deviation from normal behavior, this deviation must be due to mechanisms which are *not included* in the present SdH theory. The adequacy of the present SdH theories is thus open to question, even for the relatively simple Fermi surfaces of semimetals and semiconductors, in case of abnormal MR behavior which is not explained by intralevel scattering. This point deserves to be emphasized, since it has apparently been overlooked in the SdH literature to date—complete understanding of the field and temperature dependence of the MR is a prerequisite to valid interpretation of the SdH amplitude dependences, in *any* material. Rather than relying on the present SdH theory alone, in the case of abnormal MR behavior, one could either first understand the MR behavior and then include the responsible mechanism(s) in the SdH theory, or one could adopt the following alternative approach.

[The term MR denotes only the ordinary (nonoscillatory) magnetoresistance throughout this paper].

When the already well-understood dHvA oscillations are used to provide a basis of comparison, as discussed in Sec. I, the "normal" magnetoconductivity results, including Eqs. (2) above, may alternatively be regarded as an efficient framework within which to work toward the goal of understanding the MR oscillations. This approach is very useful because *any* MR-oscillation behavior may be efficiently described by its deviation from the normal SdH pattern. We proceed on this basis.

Before comparison with experiment, the total tensor σ^{ij} must be inverted to give the total resistivity tensor $\rho^{ij} = \rho_0^{ij} + \sum_\nu \Delta_\nu\rho^{ij}$. In general, the oscillation $\Delta_\nu\rho^{ij}$ would be expressed as a function of all eighteen quantities σ_0^{ij} and $\Delta_\nu\sigma^{ij}$. However, in the specific case of Eqs. (2) and the σ_0^{ij} which follows, a much more convenient relationship holds. For the three orientations reported in this experiment, Mg falls in the category of compensated materials with no open orbits, whose normal asymptotic field dependence is[16]

$$\sigma_0^{ij} \propto \begin{pmatrix} \beta^{-2} & \beta^{-2} & \beta^{-1} \\ \beta^{-2} & \beta^{-2} & \beta^{-1} \\ -\beta^{-1} & -\beta^{-1} & 1 \end{pmatrix} \Rightarrow \rho_0^{ij} \propto \begin{pmatrix} \beta^2 & \beta^2 & \beta \\ \beta^2 & \beta^2 & \beta \\ -\beta & -\beta & 1 \end{pmatrix},$$
(4)

with $\omega\tau = \beta$ and subject to $\omega\tau \gg 1$. In the following, only contributions to $\Delta_\nu\rho^{ij}$ of the first order in the ratio $\Delta_\nu\sigma^{ij}/\sigma_0^{ij}$ will be kept. From Eqs. (2) and (4), and from the β^{-4} dependence of each product in the determinant $\|\sigma_0^{ij}\|$, it follows that the factor $\Delta_\nu\mathfrak{N}'/\mathfrak{N}_0$ is common to all first-order contributions and that aside from the factor $\Delta_\nu\mathfrak{N}'/\mathfrak{N}_0$, the H dependence of $\Delta_\nu\rho^{ij}$ is exactly that of ρ_0^{ij} itself. This means that in analogy with Eqs. (2) the following simple equations hold:

$$\frac{\Delta_\nu\rho^{ij}}{\rho_0^{ij}} = C_\nu^{ij} \frac{\Delta_\nu\mathfrak{N}'}{\mathfrak{N}_0} = \frac{C_\nu^{ij}}{B_\nu^{ij}} \frac{\Delta_\nu\sigma^{ij}}{\sigma_0^{ij}}.$$
(5)

Here C_ν^{ij} is independent of H, but, in principle, may vary with T since relationship (4) does not fully specify the T dependence of σ_0^{ij}. This simple result means that the observable and theoretical ratios are interchangeable in work with H dependence. Equation (5), then, describes the "normal" SdH field dependence for Mg. This result [Eq. (5)] depends only on Eqs. (2) and on the fact that all six triple products in the determinant σ_0^{ij} have the same H dependence, and accordingly holds for any tensor σ^{ij} for which these conditions hold.

In order to estimate the magnitude of the observable SdH ratio (5), we differentiate the approximate relationship $\rho^{yy} = 1/\sigma^{yy}$ for compensated materials, obtaining

$$\Delta_\nu \rho^{yy}/\rho_0^{yy} = -1(\Delta_\nu \sigma^{yy}/\sigma_0^{yy})$$

or $C_\nu^{yy} = -B_\nu^{yy}$. On the basis of the spherical FS value for B_ν^{yy}, $+\frac{5}{2}$, let us suppose that the coefficients C_ν^{ij} have values of the order of 1 for real materials as well. Then it only remains to estimate the amplitude of the ratio $\Delta_\nu \mathfrak{R}'/\mathfrak{R}_0$: when corrected for the total damping factor e_r (which may be experimentally determined except for possibly the spin factor S_r), the fundamental amplitude of this ratio is twice the fraction of the total density of states lying in the ν stationary section.[11,17] For the spherical FS, this fraction is just $(1/8n)^{1/2}$[17]; for semiconductors the value will be of the order of magnitude of $(1/8n)^{1/2}$; but for the complicated many-sheeted Fermi surfaces of metals, typical values are one or two orders of magnitude less than $(1/8n)^{1/2}$. One can understand the difficulty of detecting SdH oscillations in metals, in view of their large quantum numbers n and the difficulty of measuring even the nonoscillatory resistance ρ_0^{ij} in a high-purity sample.

The observable SdH ratio $\Delta_\nu \rho^{ij}/\rho_0^{ij}$ is of course very closely related to the dHvA quantity $\Delta_\nu M_z$, since both are due to the oscillatory density of states. The component along $\vec{H}$ ($\Delta_\nu M_z$) of the oscillatory magnetization ($\Delta_\nu \vec{M}$) is given by the standard dHvA theory[11]

$$\Delta_\nu M_z = D\sqrt{H} \sum_{r=1}^{\infty} \frac{e_r}{r^{3/2}} \sin\left[2\pi r\left(\frac{F}{H}-\gamma\right) \mp \frac{\pi}{4}\right], \quad (6)$$

with all quantities evaluated at ν on the Fermi surface. Here $D = -(e\hbar\alpha/4\pi^4 m^* c)(e/c\hbar)^{1/2}(2\pi/|\alpha''|)^{1/2}$ in the conventional Gaussian cgs units for which $\omega = eH/m^* c$ holds. Equation (3) for $\Delta_\nu \mathfrak{R}'$ may now be reexpressed in terms of $\Delta_\nu M_z$,

$$\Delta_\nu \mathfrak{R}' = H^2 \left(\frac{d\ln\alpha}{d\epsilon}\right)^2 \frac{\partial}{\partial H}\Delta_\nu M_z, \quad (7)$$

where $(d\ln\alpha/d\epsilon) = \alpha^{-1}2\pi m^*/\hbar^2$. This relationship has already been derived by Pippard (1960)[18] for the less general conditions T, $T_D = 0\,°\mathrm{K}$.

The desired relationship, which is exact provided Eq. (5) is valid, is then

$$\frac{\Delta_\nu \rho^{ij}}{\rho^{ij}} = C_\nu^{ij}\frac{H^2}{\mathfrak{R}_0}\left(\frac{d\ln\alpha}{d\epsilon}\right)^2 \frac{\partial}{\partial H}\Delta_\nu M_z. \quad (8)$$

We are at present interested only in the respective fundamental amplitudes, however, so the result may be expressed more simply. Using

$$\frac{\partial}{\partial H}\sin\left[2\pi\left(\frac{F}{H}-\gamma\right)\mp \frac{\pi}{4}\right]$$
$$= -\left(\frac{2\pi F}{H^2}\right)\cos\left[2\pi\left(\frac{F}{H}-\gamma\right)\mp \frac{\pi}{4}\right]$$

and neglecting all other contributions to $\partial/\partial H\,\Delta_\nu M_z$ (which are all less than 0.002 of the one kept), we

obtain

(fundamental only): $\dfrac{\Delta_\nu \rho^{ij}}{\rho_0^{ij}}$

$$= (-)\,2\pi F\,\frac{C_\nu^{ij}}{\mathfrak{R}_0}\left(\frac{d\ln\alpha_k}{d\epsilon}\right)^2 \Delta_\nu M_z, \quad (9)$$

aside from the well-known $\frac{1}{2}\pi$ phase difference. The observable SdH fundamental is predicted to vary with H (and with T, if C_ν^{ij} is independent of T) exactly as the dHvA fundamental times the magnetoresistance ρ_0^{ij}. For the purpose of checking the theory's predictions, it is sufficient to plot $\Delta_\nu \rho^{ij}/\rho_0^{ij}\Delta_\nu M_z$, which is predicted to be flat vs H and possibly T. In addition, we divide by all other ν-dependent quantities to leave essentially only the coefficient C_ν^{ij} on the right-hand side, affording an experimental determination of the relative values of C_ν^{ij}; and we express $\Delta_\nu M_z$ as a constant times the actually measured dHvA amplitude (denoted A_ν) so that aside from a constant, the left-hand side is just the experimental ratio $\Delta_\nu \rho^{ij}/\rho_0^{ij}A_\nu$. Using $d\ln\alpha/d\epsilon = \alpha^{-1}2\pi m^*/\hbar^2$ and $\alpha^{-1} = c\hbar/2\pi Fe$, we divide by m^{*2}/F, which is the ν-dependent part of $F(d\ln\alpha/d\epsilon)^2$. The measured dHvA amplitude (A_ν) is equal to the product of $\Delta_\nu M$, $\cos_\nu\theta_c$, and G, where $_\nu\theta_c$ is the angle between $\Delta_\nu M$ and the pickup coil axis and G is an undetermined coupling constant. Also, $\Delta_\nu M_z$ equals $\Delta_\nu M\cos_\nu\theta_z$, where $_\nu\theta_z$ is the angle between $\Delta_\nu \vec{M}$ and $\hat{z}$. This yields, from Eq. (9),

$$\frac{\Delta_\nu \rho^{ij}}{\rho_0^{ij}A_\nu}\frac{\cos_\nu\theta_c}{\cos_\nu\theta_z}\frac{F}{(m^*)^2} = \frac{2\pi}{\mathfrak{R}_0}\frac{1}{G}\left(\frac{c}{e\hbar}\right)^2 C_\nu^{ij}, \quad (10)$$

and the left-hand side is the form in which the MR-oscillation data are presented. The relative heights of the predicted flat lines vs H represent the relative values of C_ν^{ij}, as a function of ν.

The dHvA data, by themselves, are presented in dHvA plots which require some discussion. As a function of T, the product of the amplitude of the dHvA fundamental and the thermal correction factor $(1/T)(e^X - e^{-X})/e^X$ varies only as e^{-X}, provided that τ_Γ^{-1} is independent of T. A log plot of this product vs T is then equivalent to a plot of $-X$ ($= -2\pi^2 kTcm^*/\hbar eH$) vs T. The slope, S, of the log plot is thus

$$S = -(2\pi^2 kc/\hbar eH)m^*,$$

which determines m^*. Since the correction factor depends on m^*, m^* must be determined self-consistently. Similarly, the theory predicts that the log plot against $1/H$, with the correction factor $H^{1/2}(e^X - e^{-X})$, should be a straight line with slope

$$S = -(2\pi^2 km^*c/\hbar e)T_D.$$

All of the dHvA data are presented graphically by these two types of plots from which the parameters

m^* and T_D are determined.

The equality of the parameters appearing in the dHvA and SdH expressions, such as m^* and T_D (or τ_Γ^{-1}), has been tacitly assumed in our treatment. That is, the correction factors of the last paragraph were assumed to cancel in the *ratio* $\Delta_\nu \rho^{ij}/A_\nu$, in Eq. (10). We note that the argument has sometimes been advanced that a difference τ_Γ^{-1}(dHvA) $\neq \tau_\Gamma^{-1}$(SdH) might be expected, in the same sample, because of the different physical manifestations of the two effects. This matter can be settled quite generally, on a theoretical basis. First, each quantized state has only one τ_Γ^{-1} (or only one lifetime τ_Γ); in particular, a view of τ_Γ^{-1} as varying over the energy width of the quantized level would not be consistent with quantum theory. Of course, τ_Γ^{-1} of the level could change with energy as the whole level shifted its position energy-wise. Second, both the dHvA and SdH theories give final expressions which are evaluated at the location ν on the Fermi energy (ζ) surface [Eqs. (2) and (6)]. Both oscillatory effects are due to the same Landau level, at the same location. Therefore, all carrier parameters observable via both effects will be identical, namely, the values precisely *at* (ζ, ν). This is in agreement with a similar statement by Pippard (1960).[19] For a genuine SdH signal, experimental field dependences characterized by T_D(dHvA) $\neq T_D$(SdH) for the same sample have occasionally been reported in the literature; possible explanations of this discrepancy are that the SdH theory that was applied to determine T_D(SdH) did not adequately describe that set of data, that the effective sample source regions differed for the two signals, or that the sample had deteriorated (or improved) between the two sets of data, by the corresponding amount. In the last two alternatives, the sample would not be the *"same* sample," from the viewpoint of quantum state lifetimes.

For later use, we should clearly state the relationship among the three rates involved in the SdH effect, and caution the reader against confusing these three rates. We distinguish between the *scattering* rate ($_s\tau^{-1}$) and the various relaxation rates which arise from it—and also between the two relaxation rates with which we are concerned in the SdH effect, namely, the *conductivity relaxation* rate τ^{-1} and the *quantum state relaxation* rate τ_Γ^{-1}. Different physical phenomena by definition involve differing relaxation processes and therefore in general have differing relaxation rates—but always defined in terms of the same given total scattering rate $_s\tau^{-1}$, of course. The rate $_s\tau^{-1}$ may include various types of scattering, such as scattering from impurities, from dislocations or strains, and from phonons. One may visualize the relationship between any given scattering rate and any particular relaxation process in terms of the concept of

effectiveness: Any given type of scattering event contributes to the relaxation rate in that process with an effectiveness ranging from 0 to 100%. Since any scattering event by definition ejects the quasiparticle out of its old state into a new state,[20] even a small-angle scattering event contributes with 100% effectiveness to τ_Γ^{-1}. In contrast, the *same* small-angle event may contribute to the conductivity relaxation rate τ^{-1} with an effectiveness of much less than 1%. Thus, one would expect that τ_Γ^{-1} would be in general greater than τ^{-1}, as is often reported in the literature. In the present experiment, the ratio $\tau_\Gamma^{-1}/\tau^{-1}$ was approximately 175, since $\omega\tau_\Gamma$ was measured to range from 2.0 to 8.58, while $\omega\tau$ characterizing the whole Fermi surface was estimated to range from 310 to 1600.

III. EXPERIMENTAL PROCEDURE

Preliminary data were taken from several samples, and the results were consistent from sample to sample. All of the data reported in this paper were then taken from one sample. The dHvA and MR oscillations were recorded simultaneously, to provide a proper basis for comparison of the two amplitudes. Thus, in contrast to previous reports in the literature, in this investigation there definitely was no alteration of the sample between the two measurements, such as may be introduced by thermal cycling. Figure 2 shows the sample geometry, including its pertinent dimensions and those of the potential probes and the unbucked dHvA pickup coil. The relative locations of these were chosen to assure, insofar as possible, that the dHvA coil would detect its signal from the same region of the sample as the potential probes (see Fig. 2). While the two source regions necessarily differ in the nature of their boundary delineations, and therefore could differ in average or effective amount of strain (i.e., in the parameter T_D), the final analysis of the experimental data indicates that the two oscillations did arise in the same effective region of the sample. The sample was kept at helium temperature during the 3-month data run, avoiding thermal cycling and the resultant generation of additional crystal imperfections, in order to assure that the sample did not change as a function of time. The initial T_D value obtained [$T_D = 0.42$ K $\pm 2.3\%$ for μ_1^5 (70°)] was repeated at the close of the run with no significant change [$T_D = 0.415$ K $\pm 2.3\%$], and the dHvA and MR oscillation amplitudes themselves were also unchanged, within experimental accuracy. The notation $\Delta_\nu \rho$ will hereafter often be used for the MR oscillations, as in Fig. 2.

The sample was oriented and cut from a high-purity magnesium single crystal, using standard x-ray and acid-string-saw techniques. No crystal imperfections were revealed when the entire source

region of the sample was examined via a large-beam x-ray exposure. The sample's current axis was within $\frac{1}{2}°$ of the $[10\bar{1}0]$ crystal axis, although the sample was tilted counterclockwise about 2° from the nominal vertical position shown in Fig. 2, with an uncertainty of $\pm 1\frac{1}{2}°$. The magnetic field rotated horizontally, from $[11\bar{2}0]$ or $\theta = 90°$ to approximately $[0001]$ or $\theta = 0°$ in Fig. 1. The sample tilt introduced no uncertainty in field orientation at $\theta = 90°$ or $[11\bar{2}0]$, and the full amount (a 3° total range) of uncertainty at the nominal $[0001]$ orientation. In the absence of any tilt, and with the y axis defined along the sample-current axis, the MR probe geometry detects primarily ρ^{yy}, plus a smaller amount of ρ^{xy} at $\theta = 90°$ or equal amounts of ρ^{xy} and ρ^{xy} at $\theta = 45°$, for example. The sample tilt has the effect of introducing small amounts of the three elements ρ^{iz} into the measured voltage. The measured voltages are, however, dominated by those elements whose normal field dependence
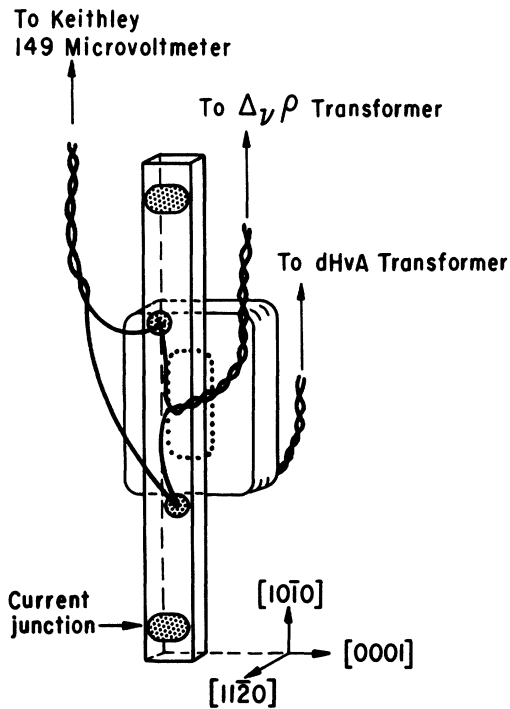

FIG. 2. Sample and the detection system (approximately to scale). The potential junctions were 0.45 mm in diameter, separated center to center by 3.37 mm along the vertical $[10\bar{1}0]$ axis and 0.40 mm along the $[0001]$ axis; and the pickup loop area enclosed by the $\Delta_{\nu}\rho$ leads was carefully minimized, as illustrated. The sample was 9.37 mm long altogether, with an approximately rectangular cross section, 0.85×0.43 mm. The 50-turn dHvA pickup coil was $3.35 \times 2.35 \times 0.69$ mm, separated from the sample by only 0.12 mm for good coupling. The current leads were soldered at the current junctions shown.

is H^2 [Eq. (4)], effectively ρ^{yy} plus an amount of ρ^{xy}. Indeed, upon field reversal it was found that the odd component of the nonoscillatory MR never exceeded 1% of the even component.

Electrical connections to the sample, through the magnesium oxide at the surface, were made by sputtering copper in an argon atmosphere, through a suitable copper mask, after the sample was freshly etched and then further cleaned by reverse-bias sputtering. These junctions were mechanically and electrically reliable with typical resistances of less than 10^{-5} Ω, copper to magnesium. Copper lead wires were then located on the copper spots, resting on chips of Cerro solder, which then melted when the sample was raised above the solder's melting point of 150 °C by the application of heat at an accessible corner of the sample. The mounting was sufficiently strain free that the sample's bulk residual-resistance ratio (RRR) at $T \leq 4.2$ K was still quite high, approximately 200 000. The mounting utilized 0.05-mm-diam (copper) potential leads and 0.075-mm current leads, because preliminary work with a similar sample showed that larger (0.2 mm) leads seriously strained that sample, lowering its bulk RRR to 25 000. The present sample's bulk RRR was estimated to be 200 000 (corresponding to $R_{4.2} = 2.2 \times 10^{-9}$ Ω) on the basis of its measured MR at helium temperatures. The latter is normally a bulk quantity, whereas surface scattering greatly exceeded bulk scattering in the sample's actual measurable zero-field resistance R, at helium temperatures. In other preliminary work, the Lorentz force resulting from the sample current (I_s) caused the sample to move, and its orientation to twist (by 3° at 10 kG and 1 A), linearly with H and with I_s. Therefore, it was necessary to "glue" one end of the sample to hold it securely at helium temperatures, yet not strain it during the thermal contraction involved in cooling down to helium temperature. This was accomplished by using Dow-Corning 200 (silicone) fluid, which was known to remain viscous to temperatures approaching those of liquid helium. The final sample was "glued down" in this manner and an upper limit of 0.001° instantaneous or short-term orientation shift due to this cause was determined, under the conditions of this experiment.

The magnetic field was produced by an electromagnet (Varian V-3800), accurate to within 1%, and homogeneous over the source region of the sample to within 1 part in 10^4. The temperature was measured to within 0.5% by standard helium-vapor-pressure techniques. The sample current source was an externally programmed Kepco power supply Model No. GK2-8M, providing the discrete currents ± 0.1, 0.2, 0.4, and 0.8 A, independent of experimental conditions to within 0.1%.
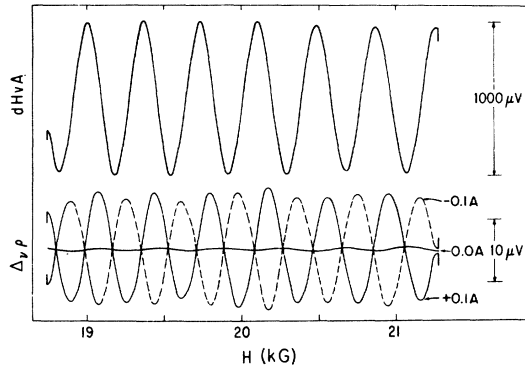
Measurement of the dHvA and $\Delta_{\nu}\rho$ amplitudes.

FIG. 3. Typical simultaneous data recording of the
dHvA and the ($I_s = 0$, ± 0.1 A) $\Delta_\nu \rho$ voltages. The data
were recorded for $\mu_1^{\vec{i}}$ (88°) at 1.37 K.

This was accomplished by techniques and instru-
mentation similar to those already described by
Stark and Windmiller[21] (SW). A frequency-separa-
tion capability such as that afforded by the large-
amplitude field-modulation technique described by
SW is required for the analysis of Mg's complicated
frequency spectrum (Fig. 1) and especially for the
still more difficult task of amplitude measurement.
Each of the two voltages was stepped up by a minia-
ture transformer in the helium bath, before the
tenth harmonic (344 Hz) of the modulation frequency
(34.4 Hz) was extracted by a phase-sensitive de-
tector (PAR model No. HR-8 with type-A input),
whose output was recorded vs H by an XY record-
er. (In effect, the tenth harmonic is a carrier
wave upon which the $\Delta_\nu \rho$ or dHvA amplitude is im-
pressed.) The two transformers were physically
separated to prevent coupling between the two pri-
mary circuits, and were shielded from all mag-
netic fields by superconducting lead foil. All am-
plitudes reported in this paper are the values mea-
sured at the lock-in detector, and may be divided
by the step-up factors, 1000 for the $\Delta_\nu \rho$ amplitude
and 600 for the dHvA amplitude, to regain the
original values.

Figure 3 shows a typical data recording, with
lock-in-detector voltages shown. The top trace is
the dHvA signal, while the bottom set of traces is
the oscillatory signal from the $\Delta_\nu \rho$ probes, at I_s
$= \pm 0.1$ A, and at $I_s = 0$. The zero-current (un-
wanted) signal is discussed later along with other
experimental phenomena and/or problems. It can
be seen that the dHvA and oscillatory magnetore-
sistance signals oscillate at identical frequencies—
the only exception to this which we observed were
some $\Delta_\nu \rho$ frequencies which were found within
about 2° of the [$11\bar{2}0$] orientation, without any ob-
servable dHvA counterpart. The beats in Fig. 3
should be noted. They are due to small amounts of
unwanted frequencies which survive the frequency

discrimination and are present in both signals.

dHvA plotted value. As shown in SW, the ex-
perimental amplitude contains the value of J_{10}, the
tenth-order Bessel function of the first kind. The
value of J_{10}, which depends on H, was experimen-
tally determined, and the measured amplitude cor-
rected for J_{10} to give the final dHvA value. The
estimated probable error of the plotted value was
never greater than $\pm 1\frac{1}{2}\%$ in the plots vs H and was
due primarily to the value of J_{10} and the factor e^X
$- e^{-X}$ discussed in the paragraph following Eq. (10).
In the plots vs T, the estimated probable errors
in the dHvA plotted values were less than 1% except
for a $\pm 2\%$ error for the lowest amplitude data
point, $\gamma_1^{\frac{1}{1}}(40°)$ at 4.2 K. The admixture of unwanted
frequencies, or amplitude beats in the recorded
signal, can cause systematic scatter of the plotted
points, in addition. Systematic errors were care-
fully considered. The major one was the changing
signal amplification as primary circuit parameters
changed with either H or T; the amplification
changed with H by less than 1% (0.2% estimated)
from 0 to 36 kG, and changed with T by $\leq 0.13\%$
over the experimental temperature range. The
transformer core's susceptibility was checked vs
T, and found to be constant from 1.1 to 4.2 K,
within an experimental uncertainty of roughly
$\pm 1\frac{1}{2}\%$, which translates into a $\pm 0.13\%$ uncertainty
in the amplification. It is mentioned in SW that
the carrier-wave skin depth must be always much
larger than the sample's dimensions, in order to
avoid skin-effect attenuation of the measured dHvA
amplitude. Since this attenuation would show up
in the dHvA plot as an increasingly rapid falloff
from the straight line toward the low-field end
(dependent on ρ_0 but not on ν) the dHvA plots them-
selves show that the effect was not present. In
addition, we determined experimentally that the
skin-depth limitation was not important for ρ_0 or
MR as low as $\frac{1}{70}$ of that at 6.05 kG at $\theta = 88°$, the
lowest value of the MR in the present dHvA and
$\Delta_\nu \rho$ plots.

Measurement of MR. The nonoscillatory MR
data were recorded along with each set of dHvA
and $\Delta_\nu \rho$ data, vs both H and T, with an estimated
relative accuracy of better than $\pm 1\%$. The MR
voltage signal was carried by twisted leads direct-
ly to a dc nanovoltmeter (the Keithley model No.
149 Milli-Microvoltmeter). A correction was
made for the dc parallel path offered by the trans-
former primary circuit. The MR data were re-
corded for both positive and negative current, typ-
ically $I_s = \pm 0.1$, ± 0.2, and ± 0.4 A; then the mag-
netic field was reversed, and the same set of data
taken again. This procedure allowed the thermo-
electric component of the voltage, as well as the
component that was odd in $\vec{H}$, to be rejected from
the MR even component which was then the final,

plotted MR value. The odd component was never larger than 1%, while the thermoelectric component never exceeded $\frac{1}{2}\%$.

Considerations peculiar to the $\Delta_\nu\rho$ amplitude. Various experimental problems were encountered in measuring $\Delta_\nu\rho$ which were not present in measuring the dHvA amplitude. Both signals were detected by the same lock-in detector, with its dials appropriately set for each signal's voltage level (typically differing by a factor of 200), and carrier-wave phase ϕ_{cw}. The modulation method of frequency separation automatically extracts the small oscillatory voltage from the much larger nonoscillatory MR voltage; the importance of this separation is illustrated by the fact that typical values of the ratio $\Delta_\nu\rho/\rho_0$ encountered in this experiment ranged from 10^{-4} to 10^{-7}. The MR does, however, act to cause a fraction of the sample current to flow through the transformer primary, requiring that the primary path have a relatively large dc resistance to prevent saturation of the transformer core.[21] The path resistance was about $0.18\ \Omega$, or 36 times the maximum MR ($5 \times 10^{-3}\ \Omega$) in the present plots.

The extremely small amplitude of the SdH oscillations presents by far the major experimental problem. One would like to take SdH data down to fields in the H^2 or normal-MR-behavior regime mentioned in Sec. II. The present low-field data were taken down to the field at which the signal-to-noise (S/N) ratio at the detector output became unacceptable, i.e., where the signal was only a few times the experimental noise value. Signal amplitudes as low as 45 nV rms at the detector input (4.5×10^{-11} V at the sample) were measured, while the estimated experimental noise below about 15 kG was constant versus field at about 17.5 nV rms at the detector input, for the detector time constant of 0.1 sec. The calculated noises at the detector input are 6 nV rms Johnson noise from the source resistance [effectively 0.18 MΩ at 1.37 K, bandwidth = $1/(4 \times 0.1$ sec$) = 2.5$ Hz]; 11 nV rms Johnson noise from the 10-MΩ detector input resistance, paralleled by the 0.18-MΩ path; and an internal detector noise of about 14 nV rms; for a calculated rms total of about 19 nV rms. Further calculation shows that either the sample temperature must be lowered to increase the signal, or else the detector's internal noise must be improved to lower the total noise, if data are to be taken to appreciably lower fields. In addition, unwanted voltages induced in the primary circuit became noticeable at about 15 kG, and by 36 kG had almost tripled the experimental noise value above. Since the dominant errors (in J_{10} and $e^x - e^{-x}$) discussed for the dHvA plots are not present in the ratio $\Delta_\nu\rho/A_{\prime\prime\prime}$ the probable error of the ratio is dominated by the $\Delta_\nu\rho$ probable error. The latter was less

than $1\frac{1}{4}\%$ except for the extreme small-amplitude data points at the lowest fields and highest temperatures, where the experimental noise caused larger errors.

The $\Delta_\nu\rho$ amplitudes showed a nonlinearity with I_s, for which a typical set of low-field values $[\mu_1^6$ ($40°$) at 16.67 kG, actually] was -2, -7, and -17% below linear, respectively, for $I_s = 0.1$, 0.2, and 0.4 A. To assure an error of no greater than 1% from this rapid amplitude loss, $\Delta_\nu\rho$ data were usually taken for three values of $(\pm)I_s$ and extrapolated to zero current, after averaging the $+I_s$ and $-I_s$ amplitude to give the amplitude at that I_s. The extrapolated or zero current amplitude was the final $\Delta_\nu\rho$ amplitude used in the plots. This extrapolation procedure completely removed the effect of the rapid amplitude loss except for some uncertainty ($\leq 1\%$) in the extrapolated value. Nonetheless, it seems wise to try to understand this nonlinearity. We have considered two explanations: I^2R heating of the sample and self-field effects. A temperature rise of the sample would cause such an amplitude loss, through the temperature damping factor. It was determined that this *was* a major cause of the amplitude loss observed above the λ point, where the helium bath is inefficient in conducting heat away from the sample and current leads. But below the λ point, at 1.37 K where the field-dependence data were taken, the field dependence of the amplitude loss was $1/H^n$ ($n > 2$) at low fields, ruling out Joule heating as an important contributor there. Instead, the amplitude-loss data at 1.37 K and low fields apparently are explained by the self-field mechanism, as follows. The magnetic self-field generated by the sample current acts to change the effective field $\vec{H}$ both in direction and magnitude, dependent upon location in the sample's cross section. Both changes alter the dHvA and $\Delta_\nu\rho$ phase, $\phi_H = 2\pi F/H$, with the direction change altering the frequency F (Fig. 1). In fact, such a phase shift was observed, especially at lower fields, proportional to I_s/H^2 within the accuracy of the data. This phase shift $\delta\phi_H$ took the form of a small sideward shift (in the x direction) of the recorded trace: at a lower field than that of Fig. 3, the zero crossings of the $\pm I_s$ traces were separated noticeably, with the $+I_s$ trace shifted in one direction and the $-I_s$ in the other; and the separation between the zero crossings, normalized by the period of the oscillation, is multiplied times π to give the experimental phase shift. A simple-model calculation, based on the phase shift due to the magnitude change δH alone, accounted for the experimental amplitude losses for all six cases, consistent within a factor of about 2 in the magnitude of δH required. If ΔH is the field interval for one full cycle of a particular signal, then δH shifts the phase by $\delta\phi_H = 360°$ ($\delta H/$

ΔH), which is proportional to I_s/H^2 because $\delta H \propto I_s$ while $\Delta H \propto H^2$. The variation over the sample of $\vec{H}$ and therefore of this self-field phase shift $\delta \phi_H$ causes an amplitude loss which is proportional to $\delta \phi_H^2$ for small $\delta \phi_H$. The experimental dependence upon both H and I_s, of both the observed phase shift and the amplitude loss (see its typical I_s dependence given above), was consistent with this model. Depending on the uniformity of the current distribution, and on the additional effect of the inhomogeneity of direction $\hat{H}$, it appears that the required values of δH (about 1.3 G at $I_s = 0.2$ A, in our simple model) would be reasonable for self-fields in the present sample. We conclude that self-fields *would* cause amplitude losses and phase shifts of roughly the observed magnitudes and dependences on I_s and H.

The *apparent* sample orientation shift due to the self-field from the sample current was rejected in determinating the maximum sample orientation shift due to the Lorentz force from the sample current. That is, all of the observed phase shifts $\delta \phi_H$ were of the instantaneous, self-field type ($\delta \phi_H \propto I_s/H^2$) within the probable error—whereas the Lorentz force would give a field-independent phase shift ($\delta \phi_H \propto I_s$). This means the probable error itself was the maximum short-term phase shift possible from the Lorentz force, converting via Fig. 1 into the maximum short-term orientation shift of $\leq 0.001°$ mentioned earlier.

Another significant phenomenon observed in some cases was a large asymmetry of the amplitude upon reversal of the current. While the $\pm I_s$ traces are *equal* in amplitude for the case in Fig. 3, in two cases the recorded $+I_s$ amplitude was noticeably greater than the $-I_s$ amplitude (the recorded traces were also shifted sideways by the above-mentioned $\delta \phi_H$ shifts, of course). For μ_1^5 (88°) the difference in amplitude upon current reversal amounted to 28% of the averaged amplitude, for $I_s = \pm 0.2$ A at 7.5 kG; this relative percentage was roughly proportional to $1/H^2$ and accurately proportional to I_s. The effect was also appreciable for λ_1^1 (88°) at lower fields. The simple arithmetical mean of the two traces was always a sinusoidal line, with amplitude proportional to I_s^2 to within experimental accuracy of a few percent. That is, the recorded amplitudes could always be resolved into two components, one linear in $\pm I_s$ and the other proportional to I_s^2, the latter giving the observed asymmetry. The quadratic component suggests thermal effects, but is equally consistent with self-field effects. Either or both explanations might help clear up this question. In any case, the asymmetric or quadratic component does extrapolate to zero relative to the linear component, leaving only the linear component in the extrapolated or zero-current amplitude. Thus, the

asymmetry has no direct effect upon the $\Delta_\nu \rho$ amplitude used.

One further complication should be mentioned. There is a dHvA-like unwanted zero-current signal whose amplitude typically was about ten times the ($I_s = \pm 0.1$ A) $\Delta_\nu \rho$ signal at the low-field end. Fortunately, the carrier waves of the $\Delta_\nu \vec{M}$ and $\Delta_\nu \rho$ signals in the sample are in phase (see SW), so that the dHvA-carrier-wave signal *induced* in any pickup coil is 90° out of phase with the $\Delta_\nu \rho$ signal. The carrier-wave phase (ϕ_{cw}) of the unwanted signal in the $\Delta_\nu \rho$ leads was just that of the true dHvA signal, within the experimental accuracy of $\leq 5°$. Thus the $\Delta_\nu \rho$ data could be taken at the detector ϕ_{cw} phase setting where the unwanted signal was, in principle, zero. In practice, a small unwanted null signal remained and was recorded as the ($I_s = 0$) zero-current trace, Fig. 3. We note that as the sample current causes the phase vs H of every oscillatory signal to shift (by the $\delta \phi_H$ shift discussed earlier), the effect of I_s upon the unwanted signal is to slide it sideways on the recorder chart, and the result is as if a bona fide $\Delta_\nu \rho$ signal due to I_s had been *added* to the zero-current unwanted signal. This spurious signal is in principle indistinguishable from the actual $\Delta_\nu \rho$ signal for any set of recorder traces such as $I_s = \pm 0.1$ A, 0, at a given detector setting ϕ_{cw}. The conceivable possibility that the sample current was somehow generating an unknown I_s signal by some other mechanism required careful investigation. Extensive data were taken at a variety of detector settings, ϕ_{cw}, and all traces were found to be completely consistent with a self-field phase shift $\delta \phi_H(I_s)$ of the observed zero-current signal plus a $\Delta_\nu \rho$ signal. We concluded that the only bona fide I_s signal was the $\Delta_\nu \rho$ signal, at the correct $\Delta_\nu \rho$ carrier wave phase ϕ_{cw} (90° away from ϕ_{cw} of the dHvA signal), and that no unknown mechanism was indicated. The small zero-current signal remaining as in Fig. 3 still caused a small spurious I_s signal, introducing a $\Delta_\nu \rho$ amplitude uncertainty of nearly always less than 1%, and always considerably less than the uncertainty due to noise.

The possibility should also be mentioned that the oscillating Lorentz force (due to the oscillating modulation field) can vibrate the sample and cause a spurious vibration $\Delta_\nu \rho$ signal due to the dHvA-like zero-current signal; in fact, an *unglued* preliminary sample gave vibration $\Delta_\nu \rho$ signals which were larger than the genuine $\Delta_\nu \rho$ signals. The oscillatory sample orientation may be written $\theta = \theta_0 + \theta_1 \cos(\omega t - \delta)$, where $\theta_1 \leq 10^{-3}$ deg for the present glued sample and the phase lag δ would be zero if there were no damping. The formulation of the effect is then quite analogous to that of the dHvA signal itself (see SW), except that a portion $\sin \delta$ of the signal appears at the $\Delta_\nu \rho$ carrier-wave phase ($\cos \delta$ of the signal remaining at the dHvA phase).
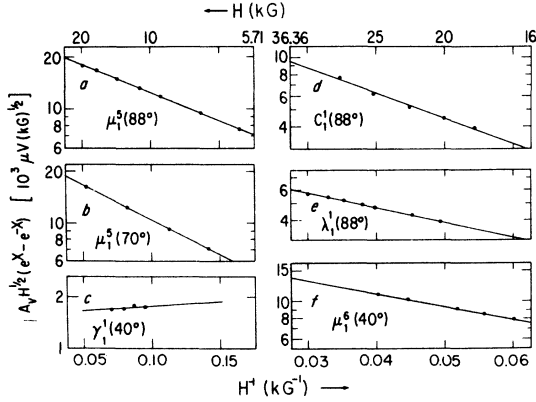
FIG. 4. dHvA log plots vs H^{-1}, at 1.37 K. The six orbits are grouped into a low-frequency group (a–c, in the field range 6–20 kG) and a high-frequency group (d–f, in the higher-field range 16–35 kG).

Calculation of the amplitude shows that for θ_1 $\leq 0.001°$ the vibration $\Delta_\nu\rho$ signals could not have exceeded 0.1% of the measured $\Delta_\nu\rho$ signals.

The exact nature of the zero-current signal was not investigated in detail, but its field dependence was noticeably different from the dHvA field dependence. For λ_1^1 (88°), the amplitude increased over the given field range by about 30% *less* than the dHvA increase, while μ_1^5 (70°) showed a 55% *larger* increase. This signal apparently did not otherwise differ from a true dHvA signal: The signal's detector phase ϕ_{cw} was approximately correct for an induced signal, differing by $\leq 5°$ from the

true dHvA signal's phase. Also, the amplitude was about $\frac{1}{100}$ of the dHvA amplitude induced in the 50-turn dHvA pickup coil, which is reasonably consistent with a dHvA signal induced in the unavoidable loop area presented by the $\Delta_\nu\rho$ leads (Fig. 2) due to the finite thickness of the sample. The simplest possibility is that the zero-current signal resulted from the dHvA signal aided or opposed by an unknown signal of differing field dependence, and that the latter signal was generated somehow by the modulation field or the induced eddy currents in the sample. Two other features which perhaps play a part are the fact that the sample is in electrical contact with the detection circuit, and the fact that the sample itself is part of the detection circuit. Possibly the dHvA signal is modified by these features of its pickup loop, in such a way as to result in the field dependences mentioned above. For example, the sample's MR variation with H may conceivably cause the pickup loop area to vary with H by the above percentages.

IV. RESULTS AND DISCUSSION

A. As a Function of H

dHvA Plots

The dHvA plots (Fig. 4) use the effective masses obtained from the plots vs T, and their slopes determine the parameter T_D [$S = -2\pi^2 kcm^*(\hbar e)^{-1}T_D$], as discussed in Sec. II. In three of the six cases, MB introduces an extra field dependence, so that if the slope is converted to a temperature (T_S), its value differs from the T_D value. For γ_1^1 (40°) and μ_1^6 (40°) we have calculated the appropriate MB

TABLE I. dHvA slope value T_S and the dHvA parameter T_D for each extremal orbit ν; the parameters F and m^*; and the field ranges over which the $\Delta_\nu\rho$ data were taken together with the corresponding ranges of n, X_D, and $\omega\tau_\Gamma$.

ν	μ_1^5 (88°)	C_1^1 (88°)	λ_1^1 (88°)	μ_1^5 (70°)	γ_1^1 (40°)	μ_1^6 (40°)
T_S(K)	0.358 ± 0.010	0.741 ± 0.031	0.315 ± 0.014	0.420 ± 0.013	-0.063 ± 0.030	0.322 ± 0.013
T_D(K)	0.358 ± 0.010	0.4[a]	0.315 ± 0.014	0.420 ± 0.013	0.61[a]	0.49[a]
$F(10^6$ G)	2.70	7.78	27.2	2.88	2.85	16.39
$m^*(m_0)$	0.141	0.307	0.424	0.151	0.127	0.366
H range (kG)	6.05 to 20.1$_8$	17.0$_3$ to 29.4$_7$	20.3$_3$ to 35.4$_0$	6.68 to 18.9$_5$	10.0$_2$ to 15.6$_7$	16.4$_9$ to 25.2$_4$
n range	446 to 134	457 to 264	1340 to 768	431 to 152	284 to 182	994 to 650
X_D range	1.22 to 0.366	1.06 to 0.61	0.843 to 0.484	1.40 to 0.492	1.14 to 0.73	1.60 to 1.04
$\omega\tau_\Gamma$ range	2.57 to 8.58	3.0 to 5.1	3.73 to 6.49	2.25 to 6.38	2.8 to 4.3	2.0 to 3.0

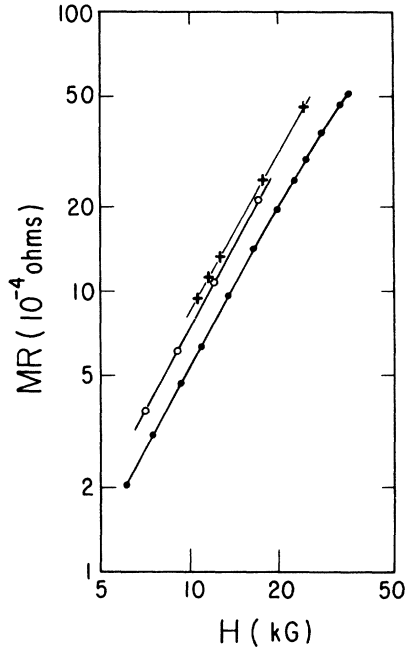[a]Obtained by correcting for known effects of magnetic breakdown (see text).

FIG. 5. Magnetoresistance vs H on a log-log plot at 1.37 K. The field dependence is $H^{1.87}$ at the orientation 40° (crosses), $H^{1.92}$ at 70° (circles), and ranges from $H^{1.95}$ down to about $H^{1.45}$ at 88° (dots).

correction factor,[3] and the corrected data point plots deviate from a straight-line fit by $\leq 1\frac{1}{2}\%$, or approximately the probable error. These plots determine T_D, and the T_S and T_D values are presented in Table I, along with other collected parameters for all six cases. For the remaining MB case C_1^1 (88°), the T_D value (0.4 K) was simply chosen to lie within the range of values of the other five cases, as it plausibly would be. The MB parameter[3] H_0 used in the calculation for γ_1^1 (40°) and μ_1^6 (40°) was varied from 5.8 kG to $5.8/\cos 40° = 7.6$ kG, giving the following variation of T_D values (the average value is presented in Table I), respectively: for γ_1^1 (40°), $T_D = 0.64-0.58$ K; for μ_1^6 (40°), $T_D = 0.495-0.485$ K.

Magnetoresistance Plots

The MR data vs H are presented in Fig. 5 in the form of log-log plots, whose slopes directly display the exponent of H in $MR \propto H^n$. At all three orientations, the field dependence is below the "normal" H^2 behavior, in the field range observed. Thus, as noted earlier, the present SdH theories may fail to describe the field dependence of even a pure SdH oscillation in this field range. Therefore, let us consider some possible causes of the MR field dependences in Fig. 5, preparatory to consideration of the field dependence of the MR oscillations.

(i) One possible cause is magnetic breakdown.

The following case is sufficient to illustrate this mechanism. For $\omega\tau \gg 1$ and for the case of isotropic elastic scattering, the transverse element σ^{yy} may be written[22] in terms of the density of states differential $d\mathfrak{N}_\alpha$ for an orbit α contained in the dk_z slice,[23] as an integral over the FS density of states,

$$\sigma^{yy} = \frac{c^2\hbar^2}{H^2} \int \sum_\alpha d\mathfrak{N}_\alpha \langle (k_x - \bar{k}_x)^2 \rangle_\alpha \tau^{-1}. \tag{11}$$

Here $\tau^{-1}(\zeta) = \int \sum_\alpha d\mathfrak{N}_\alpha P(\zeta) \equiv \mathfrak{N}(\zeta)P(\zeta)$,[24] the product of the total FS density of states and the conventional isotropic elastic scattering quantity $P(\zeta)$.[24] Also, $\langle k_x \rangle_\alpha = \bar{k}_x$ is the average of k_x over the α orbit—so that the contribution to (11) from the dk_z slice of the FS is proportional to the mean-square k_x orbit dimension, averaged over all orbit states in the slice. This expression is valid for any carrier orbit α, including MB-coupled orbits when the density-of-states differential element $d\mathfrak{N}_\alpha$ is appropriately expressed.[25] If the probability of larger coupled orbits increases as the MB probability increases, then the mean-square k_x orbit dimension and hence the integral (11) will increase, above its normal H^{-2} field dependence. Thus MB may cause the observed MR field dependences. Its possible effects on the ratio $\Delta_\nu\rho/\rho_0$ for even pure SdH oscillations will be discussed later.

(ii) Intralevel scattering is a second mechanism which may contribute significantly to the observed MR field dependence. As mentioned earlier, for pure isotropic elastic scattering the contribution would be negligible ($\leq 0.55\%$), essentially because there is very little intralevel scattering at large quantum numbers for this scattering case. For realistic scattering, however, this mechanism cannot be ruled out.

(iii) A third possible contribution to the observed MR field dependence should be included: Transport theory ordinarily considers only the bulk, ignoring the sample surfaces. However, the element σ^{yy}, being linear in τ^{-1}, may be much larger in the surface layer than in the bulk, as a result of the surface scattering contribution to τ^{-1}. This gives rise to surface sheath current flow, which becomes important whenever the conductivity bulk mean free path (mfp) approaches the sample cross-section dimensions. We can estimate the effective bulk mfp as the product of the bulk relaxation time and an average velocity. From Table I we take $T_D = 0.4$ K as a representative value of T_D, which corresponds to $\tau_r = 3.04 \times 10^{-12}$ sec. Since τ is of the order of $175\tau_r$ ($= 5.3 \times 10^{-10}$ sec), and v_F is about 3×10^8 cm/sec, the estimated mfp is 1.6 mm. This is several times the sample's cross-section dimensions, 0.43×0.85 mm. Thus, it is likely that significant current was caused to flow near the surfaces of the sample, and such sheath current

might have contributed significantly to the MR field dependence.

$\Delta_\nu \rho$ *Plots*

For a given ν, each plotted point in Figs. 6 and 7 [see Eq. (10)] consists of the measured ratio $\Delta_\nu \rho / \rho_0 A_\nu$ multiplied by two constants $F_\nu (m_\nu^*)^2$ and $\cos_\nu \theta_c / \cos_\nu \theta_z$. The values of F_ν and m_ν^* (Table I) were measured by the standard dHvA procedures, and F_ν agrees with Stark's accurate values[8] for F_ν to within 1%, while the m_ν^* values are also within experimental error of previously published data. Determination of the second factor is a matter of calculation of the direction of the vector $\Delta_\nu \vec{M}$, for a given field orientation $\hat{z}$ and with the pickup coil axis fixed along the $[11\bar{2}0]$ axis of the sample. These directions are all in the plane of field rotation and are thus specified by the values θ_ν, which are presented in Table II along with the values $\cos_\nu \theta_c / \cos_\nu \theta_z$. For $\lambda_1^1 (40°)$ as an example, $\theta_\nu = 5.0°$ and the desired ratio is $\cos(90° - 5°)/ \cos(40° - 5°) = 0.107$. It should be emphasized that the data ratio $\Delta_\nu \rho / \rho_0 A_\nu$ may readily be recovered from the plots of Figs. 6 and 7. The log plots of the data ratio $\Delta_\nu \rho / \rho_0$ may be obtained by simply adding the slope of the corresponding dHvA plots
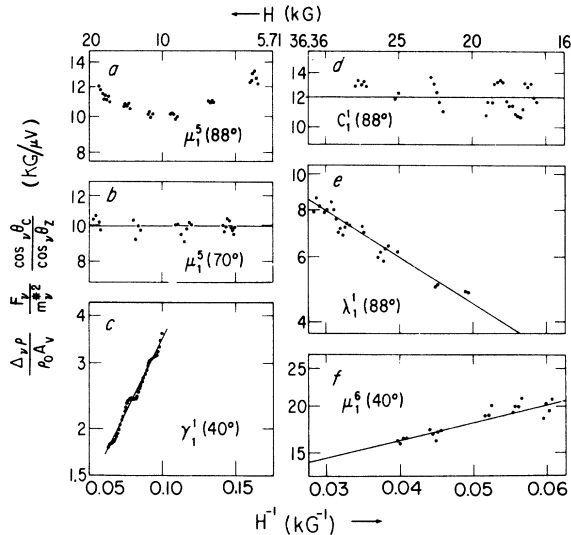
TABLE II. Calculated angle θ_ν of $\Delta_\nu \vec{M}$ and the factor $[\cos_\nu \theta_c / \cos_\nu \theta_z]$.

ν	μ_1^5 (88°)	C_1^1 (88°)	λ_1^1 (88°)	μ_1^5 (70°)	γ_1^1 (40°)	μ_1^6 (40°)
$\theta_\nu(°)$	90.22	88.5	88.4	92.5	5.0	58.2
	±0.22	±0.5	±0.4	±1.0	±0.5	±1.2
$\dfrac{\cos_\nu \theta_c}{\cos_\nu \theta_z}$	1.00	1.00	1.00	1.08	0.107	0.897
				±0.01	±0.010	±0.018

(Figs. 4 and 8), and the absolute value of $\Delta_\nu \rho / \rho_0$ may be obtained by multiplying the recovered $\Delta_\nu \rho / \rho_0 A_\nu$ value by the corresponding dHvA amplitude recovered from its own plot. Similarly, the $\Delta_\nu \rho$ log plots and absolute values may be obtained using the ρ_0 data, Figs. 5 and 9. As mentioned earlier, this measured value of $\Delta_\nu \rho$ is divided by the step-up factor of 1000 to give the actual value at the sample.

The systematic oscillatory patterns in Fig. 6 are the dominant cause of uncertainty in determining the exact field dependence. These oscillations result from beats in the data, due to the admixture of unwanted frequencies. The appropriate way to handle this problem is to either use additional frequency discrimination (see SW[21]) or to average over more data points. Thus, for the γ_1^1 case the data blanketed the complete field range, and the ratio $\Delta_\nu \rho / \rho_0 A_\nu$ was averaged over 25 cycles of the γ_1^1 oscillation before being plotted in Fig. 6. The surviving beat frequency in this plot is about 0.077 $\times 10^6$ G, $\frac{1}{37}$ of γ_1^1's frequency (2.85 $\times 10^6$ G), and probably is due to the fourth harmonic of μ_1^1, with frequency $\frac{1}{37}$ below γ_1^1's frequency. The fact that such admixture oscillations, Fig. 6, scarcely show up in the dHvA plots (merely causing the $\pm 1\frac{1}{2}\%$
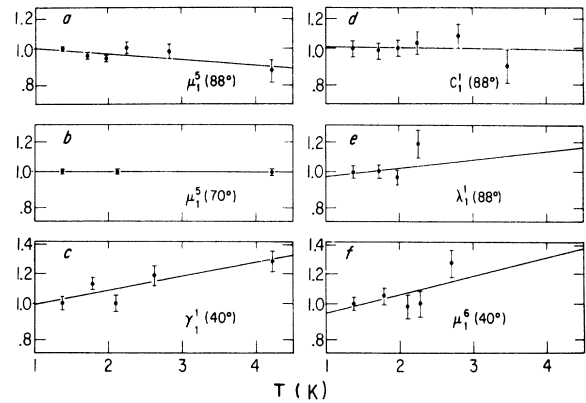

FIG. 6. $\Delta_\nu \rho / (\rho_0 A_\nu)$ log plots vs H^{-1}, at 1.37 K, with the six orbits arranged as in Fig. 4. The probable errors of the plotted points were less than $\pm 1\frac{3}{4}\%$, except for the extremely small-amplitude points at the lowest fields, where the probable errors were as follows, due chiefly to the experimental noise: $\pm 5\%$ for the lowest field cluster of points in (a); $\pm 4\%$ for the lowest cluster in (b); and $\pm 2\frac{1}{2}$ and $\pm 5\%$ for the two lowest clusters in (e). The admixture of unwanted frequencies caused the oscillation in (c) as well as the more complicated oscillation patterns in the other plots and clearly dominated the uncertainty in shape and slope of the plots.

FIG. 7. $\Delta_\nu \rho / (\rho_0 A_\nu)$ log plots vs T, at the fields specified in Fig. 9, plotted as a fraction of (i.e., normalized to) the 1.37 K value. The probable error bars at 1.37 K were estimated on the basis of the Fig. 6 uncertainties at the specified fields, and the probable errors at higher temperatures were estimated similarly.
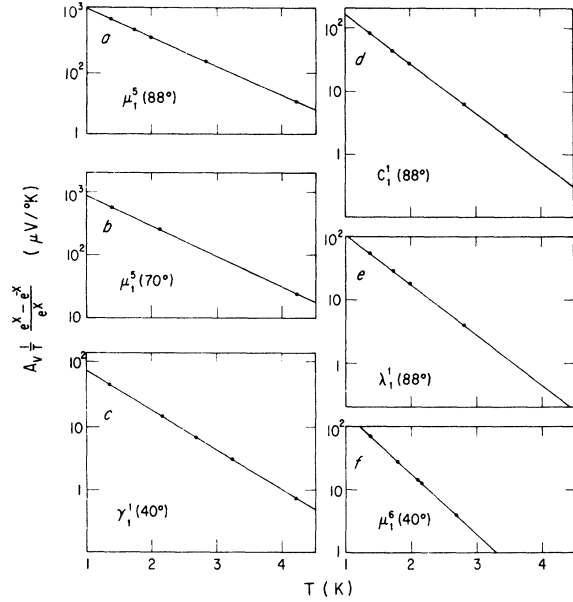
FIG. 8. dHvA log plots vs T, at the Fig. 9 fields. There is no apparent deviation from a straight line dependence.

FIG. 9. Magnetoresistance MR vs T plotted as a percentage change from its 1.37 K value. The curves shown have the form, $R(T) = R(0 \text{ K})/(1 + cT^3)$ [Eq. (12) in the text], fitted to the two end data points for each case.

scatter in the γ_1^1 dHvA plot, for example) is consistent with the known lower harmonic content of dHvA oscillations [Eq. (6)] compared with SdH oscillations [Eq. (2)]. The intralevel scattering contributions not contained in Eq. (2) also increase or enhance the harmonic content of the SdH oscillation beyond that given by Eq. (2).[13,14] In addition, interference frequencies are generated in $\Delta\rho^{ij}$ by two mechanisms not present in the dHvA oscillations, and this is an additional source of unwanted frequencies in the MR oscillation data. One mechanism is large angle scattering between any two extremal orbits, generating combination frequencies in σ^{ij}; the other is the neglected second-order terms which are generated in the inversion of σ^{ij} to give ρ^{ij}.

It should be pointed out that interference frequencies and higher harmonics, being strong enough to cause the present admixture problem, are also
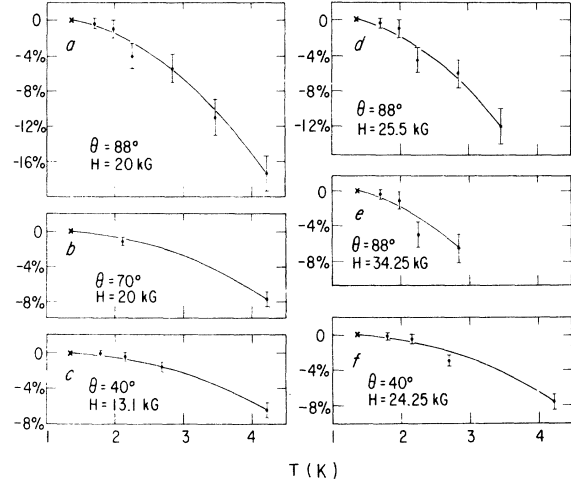
strong enough to be quite readily investigated, in future MR oscillations work with high-purity materials.

The values of the slopes in Fig. 6 are presented in Table III, interpreted as temperatures (T_S) exactly as for the dHvA plots. When this slope value (top line) is added to the T_S value (second line) for the corresponding dHvA plot, then the T_S slope value for the dHvA-like plot of $\Delta_\nu\rho/\rho_0$ is obtained (third line). Except for μ_1^5 (88°), each of the latter plots would have an apparently straight-line field dependence. Thus, if an experimentalist had plotted the standard $(\Delta_\nu\rho/\rho_0)$ plots without any simultaneous dHvA data, he might have applied the current SdH theory and interpreted the slopes of his plots as T_D's. Some of the errors made thereby would have greatly exceeded 100% of the true T_D's, included in Table III (bottom line) for comparison.

From Fig. 6 one sees that the six C_ν^{ij}'s, in the sense of an average value for each plot, are not extremely different in value. This is consistent with the assumption that the SdH mechanism actual-

TABLE III. Three slope parameters T_S and the parameter T_D in K.

ν	μ_1^5 (88°)	C_1^1 (88°)	λ_1^1 (88°)	μ_1^5 (70°)	γ_1^1 (40°)	μ_1^6 (40°)
$T_S\left(\dfrac{\Delta_\nu\rho}{\rho_0 A_\nu}\right)$	$\begin{bmatrix} -0.280 \\ \text{to} +0.373 \end{bmatrix}$	0.0 $+0.045$ -0.000	0.467 ± 0.024	0.0 ± 0.008	-0.963 ± 0.010	-0.189 ± 0.019
T_S (dHvA)	0.358	0.741	0.351	0.420	-0.063	0.322
$T_S\left(\dfrac{\Delta_\nu\rho}{\rho_0}\right)$	$\begin{bmatrix} 0.078 \\ \text{to} \ 0.731 \end{bmatrix}$	0.741	0.782	0.420	-1.026	0.133
T_D	0.358	0.4	0.315	0.420	0.61	0.49

ly was an important contributor to the present six "SdH" oscillations. By contrast, the value of $C_\nu^{ij}(\nu = \mu_1^5)$ within $\pm 0.1°$ of the $[11\bar{2}0]$ axis was at least 40 times greater than the maximum value in Fig. 6—the MR oscillation near $[11\bar{2}0]$ clearly must have been due primarily to a different, stronger mechanism.

Field Dependences

The field dependences in Fig. 6 are definitely not the normal flat plot dependences predicted by Eq. (10), for four of the six cases, and we shall consider various possible explanations below. For only two cases, the non-MB orbit μ_1^5 (70°) and the MB orbit C_1^1 (88°), can the data plots be flat, within the uncertainty in shape and slope of the plots.

(i) First, the possibility that $T_D(\text{SdH})$ was different from $T_D(\text{dHvA})$ due to different source regions for the two effects, discussed earlier, would give either $T_D(\text{SdH}) > T_D(\text{dHvA})$ for all cases (producing a positive slope toward higher field for all cases), or else the opposite situation for all cases—whereas there are slopes of both signs in Fig. 6. Even though this mechanism cannot account for the observed field dependences, it plausibly could have introduced a slope as large as the slope uncertainty for μ_1^5 (70°), say. This corresponds to $T_D(\text{SdH})$ differing from $T_D(\text{dHvA})$ by only 2%. On this basis, it is unlikely that the source regions for the two effects were very different.

(ii) Second, more experimental work involving other probe geometries should be done to sort out the various ρ_0^{ij} and $\Delta_\nu\rho^{ij}$ tensor components which were present at the given probes. We feel that ρ^{yy} primarily determined the reported signals, and that similar behavior would have been observed for it alone, but this cannot be concluded with certainty without further work.

(iii) Let us consider the effect of MB, occurring elsewhere on the FS (at a value of k_z different from ν) upon the field dependence of any MR oscillation arising at the extremal orbit ν and due only to the SdH mechanism. The effects arising from MB occurring exactly at the ν orbit will be considered separately (later). That is, let us see what behavior a SdH theory extended to cover this situation would predict. We shall use the simple relationship

$$\Delta_\nu\rho^{yy}/\rho_0^{yy} = C(\Delta_\nu\sigma^{yy}/\sigma_0^{yy}),$$

which allows interchanging of the two ratios, so that we may simply consider the ratio $\Delta_\nu\sigma^{yy}/\sigma_0^{yy}$. This relationship (with $C = -1$) follows from $\rho^{yy} = 1/\sigma^{yy}$, which should be a plausible first approximation even in the presence of abnormal field dependences, for compensated materials. From Eq. (11) for σ^{yy}, one can see that the oscillation $\Delta_\nu\sigma^{yy}$ arises from the density of states oscillation

in two ways: directly from $d\mathfrak{N}_\nu$ in $\sum_\alpha d\mathfrak{N}_\alpha$, and indirectly through the scattering part of σ^{yy}—e.g., from $d\mathfrak{N}_\nu$ in $\tau^{-1} = \int\sum_\alpha d\mathfrak{N}_\alpha P(\zeta)$ for isotropic elastic scattering. Since MB does not affect the nonoscillatory part of τ^{-1} [$\tau_0^{-1} = \mathfrak{N}_0(\zeta)P(\zeta)$ is independent of MB], the part of $\Delta_\nu\sigma^{yy}$ coming directly from $d\mathfrak{N}_\nu$ is not at all affected by any MB process occurring elsewhere on the FS. As σ_0^{yy} increases by $X\%$ due to the MB mechanism discussed following Eq. (11), the scattering part of $\Delta_\nu\sigma^{yy}$ does however increase, by the same $X\%$ in the case of isotropic elastic scattering. It follows that the ratio $\Delta_\nu\rho/\rho_0$ decreases by an amount varying from 0 to $-X\%$, due to MB occurring elsewhere on the FS. For general scattering, much larger changes in the scattering fraction of $\Delta_\nu\sigma^{yy}$ are possible. If ν were situated very near an MB location whose local conductivity contribution $d\sigma^{yy}$ were greatly increasing or decreasing—and if the scattering part of $d\sigma^{yy}$ were due to small angle scattering so that the nearby density of states $d\mathfrak{N}_\nu$ dominated in it—then while the total σ_0^{yy} increased by $X\%$, $\Delta_\nu\sigma^{yy}$ could conceivably increase or decrease by any percentage, corresponding to the increase or decrease of the local $d\sigma^{yy}$ at the MB location. Thus, except when the change in $\Delta_\nu\sigma^{yy}$ happens to be exactly equal to the change in σ_0^{yy}, MB causes a deviation from the normal field dependence predicted by the current SdH theory for the ratio $\Delta_\nu\sigma^{yy}/\sigma_0^{yy}$, whenever it causes any deviation of σ_0^{yy} from its normal H^{-2} dependence. Actual determination of the net result for the three MB orbits, for general scattering, is beyond the scope of this paper, but the large percentage decreases for γ_1^1 (40°) and μ_1^6 (40°) in Fig. 6 might be due to this mechanism— this is a possibility which must be considered. The non-MB orbits λ_1^1 and μ_1^5 are known to be distant from any MB location, however, so it is unlikely that small angle scattering couples any MB locations more closely to the λ_1^1 and μ_1^5 orbits than to an average FS orbit. That is, the isotropic scattering results should be a good approximation and this mechanism probably does not explain the large percentage changes for λ_1^1 (88°) and μ_1^5 (88°) in Fig. 6.

The Fig. 5 MR decrease below H^2 behavior was about 8% over the μ_1^5 field range at $\theta = 70°$, so a few percent decrease could be expected in the Fig. 6 plot for μ_1^5 (70°), if the 8% decrease was due to MB. If so, the decrease was hidden within the slope uncertainty of the μ_1^5 (70°) plot or was approximately cancelled by other changes, or both.

(iv) The other two MR mechanisms—sheath current flow and intralevel scattering—might be capable of explaining all of the abnormal plots in Fig. 6. However, theoretical work is needed before any definitive statement can be made concerning the effects of sheath current flow. As mentioned

earlier, we do know that isotropic elastic intra-
level scattering increases the SdH amplitude by
less than 1%, which cannot explain the field depen-
dences in Fig. 6. Realistic intralevel scattering,
however, cannot be ruled out as a possible explana-
tion of the observed behavior.

At this point, before consideration of two *non-*
SdH MR-oscillation mechanisms [(v) and (vi), be-
low], we can conclude the discussion of μ_1^5 ($70°$),
the one case which definitely is a nearly pure SdH
MR oscillation. If we adopt the simplest possibili-
ty, that two or more of the above mechanisms
[(i)–(iv)] did not cancel each other, then the ex-
perimental evidence in Fig. 6 imposes an upper
limit of at most a few percent deviation from nor-
mal SdH behavior, due to any one of the above
mechanisms. Further experimental work would,
however, be desirable to determine the extent or
size of any deviations from normal SdH behavior
over wider field ranges for this and other pure
SdH cases.

(v) The contribution of non-SdH mechanisms
[(v) and (vi)] to the observed MR oscillations could
account for all of the abnormal experimental field
dependences. A new non-SdH mechanism definite-
ly exists within $\pm 0.1°$ of [$11\bar{2}0$], and may contribute
significantly at the nearby orientation $\theta = 88°$, where
MR is still steeply changing with θ. Roughly the
same [$11\bar{2}0$] behavior was observed for all frequen-
cies checked, for both MB (C_1^1) and non-MB orbits—
the MR oscillation magnitude increases on the or-
der of forty-fold while the MR value decreases
only 30% within an interval of $0.1°$ as the [$11\bar{2}0$]
orientation is approached. This definitely is not
the large amplitude MB-oscillation mechanism
since neither the C_1^1 orbit nor the non-MB orbits
take part in the pertinent MB key process discussed
earlier. It appears that these MR oscillations are
caused by the dHvA oscillations, which are in $\vec{B}$
and thus cause $\rho^{yy} = f(\vec{B})$ to oscillate vs H—here $\vec{B}$
is the field which actually exists in the sample,
otherwise set equal to the external field $\vec{H}$ through-
out this paper. (The difference between this effect
and the well-known Shoenberg effect is that here
the $\Delta_\nu \vec{B}$ dHvA oscillations act upon the MR, while
in the Shoenberg effect they act self-consistently
upon themselves.) This dHvA or $\Delta_\nu \vec{B}$ mechanism
clearly generates strong MR oscillations wherever
the MR is a very steep function of orientation, in
agreement with our observations and the previous
observations by Young in tin.[26] According to our
preliminary calculations, the ratio $\Delta_\nu \rho / \rho_0 A_\nu$ is
predicted to increase by large percentages toward
lower fields, in contrast to the normal flat behav-
ior. This is in agreement with our observations
near [$11\bar{2}0$], and appears to explain the low-field
μ_1^5 ($88°$) behavior. Whether or not this mechanism
is pertinent to the high-field μ_1^5 ($88°$) and λ_1^1 ($88°$)

behavior depends upon the exact phase vs H (ϕ_H) of
the MR oscillation. This phase ϕ_H should be exact-
ly that of $\Delta_\nu \vec{M}$ itself, and should therefore differ by
exactly $90°$ from ϕ_H of the pure SdH oscillation,
when only the fundamental harmonic is considered.
A phase difference with effective value greater
than $90°$ is at least conceivable, however. In that
case this contribution could partially cancel the
normal SdH contribution, which would produce field
dependences such as observed for λ_1^1 ($88°$) and μ_1^5
($88°$) in Fig. 6. It may be relevant that the unex-
plained asymmetry in $\pm I_s$ was for these two cases.
On the basis of the steepness of the MR vs θ, it is
likely that this mechanism contributed significantly
to all cases at $\theta = 88°$ but was unimportant at $\theta = 70°$
and $\theta = 40°$.

We conclude that the $\Delta_\nu \vec{B}$ mechanism (v) probably
explains the low-field μ_1^5 ($88°$) behavior, while
mechanisms (iv) and (v) are the most likely explana-
tions of the λ_1^1 ($88°$) and high-field μ_1^5 ($88°$) behav-
ior. This completes our consideration of the three
non-MB orbits.

(vi) A second non-SdH MR-oscillation mechanism
should be important for the three MB orbits—in
addition to the effects already considered, (i)–(v).
The isotropic elastic scattering case, Eq. (11), is
sufficient to demonstrate the existence of this (MB-
oscillation) mechanism for all MB extremal (ν)
orbits. All of the carrier orbits α which are cou-
pled to the ν orbit by MB define an MB-coupled-
orbit group of carriers, whose mean-square k_x
orbit dimension changes as the MB probability in-
creases. But also, as for the large amplitude MB
oscillation discussed earlier (see Ref. 3), the
probability of transition across any MB junction
(say from orbit α to orbit β) is proportional to the
probability for the carrier to be at the MB junction
initially (and therefore $d\mathfrak{N}_\alpha$) and to the final density
of states ($d\mathfrak{N}_\beta$). Thus, the probability of transition,
and therefore the distribution of the given group of
carriers over the various possible coupled orbits,
oscillates at the frequency F_α of each orbit α. In
this sense, the two MB-oscillation mechanisms
differ primarily in amplitude: if the given carrier
group is causing the MR category to change, *large
amplitude* oscillations result, with values of C_ν^{ij}
which typically are $100-10^4$ times larger than any
values in Fig. 6. In Eq. (11), then, as the distri-
bution of carriers oscillates the mean-square k_x
orbit dimension oscillates and is now added to the
SdH sources of oscillation $d\mathfrak{N}_\nu$ and τ^{-1}. That is, the
oscillation of $d\mathfrak{N}_\nu$ gives rise to the oscillation of
(11) *indirectly*, through the contribution $\sum_\alpha d\mathfrak{N}_\alpha \langle (k_x - \bar{k}_x)^2 \rangle_\alpha$ of the whole group of carriers, as well as
indirectly through τ^{-1} and directly by virtue of $d\mathfrak{N}_\nu$
in $\sum_\alpha d\mathfrak{N}_\alpha$. It should be mentioned that the extra
MB field-dependent factor calculated earlier for
the dHvA amplitude for the MB orbits is also pres-

TABLE IV. Effective mass m^* in units of m_0.

	μ_1^5 (88°)	C_1^1 (88°)	λ_1^1 (88°)	μ_1^5 (70°)	γ_1^1 (40°)	μ_1^6 (40°)
m^* (dHvA)	0.141 ± 0.002	0.307 ± 0.005	0.424 ± 0.010	0.151 ± 0.003	0.127 ± 0.002	0.366 ± 0.008
m^* (cyclotron resonance)[a]	0.140[b] ± 0.004	0.306 ± 0.006	0.422 ± 0.004	c	0.127 ± 0.003	c
$\dfrac{m^*(\Delta_\nu\rho)}{m^*(\text{dHvA})}$	1.03 ± 0.02	1.00 ± 0.02	0.97 ± 0.06	1.00 ± 0.00	0.94 ± 0.03	0.95 ± 0.03

[a]Values from Fig. 2 of Ref. 25.
[b]Their μ_1^5 (90°) value.
[c]Not observed in Ref. 25.

ent in the MR oscillation from all three sources. Within the approximation that the MB probability is independent of energy ϵ, made in Ref. 3, this factor must be the same in *all* quantum oscillatory effects since it appears in $d\mathfrak{N}_\nu$,[3] the ultimate source of all such effects. This extra MB factor therefore must cancel out of the ratio $\Delta_\nu\rho/A_\nu$ and accordingly cannot contribute to the abnormal behavior in Fig. 6.

The γ_1^1 (40°) and μ_1^6 (40°) decreases in Fig. 6 can be explained on the basis of this MB-oscillation contribution to $\Delta_\nu\sigma^{yy}$ if this contribution is decreasing relative to the normal SdH oscillation, with the two contributions differing in phase ϕ_H by less than 90°. Alternatively, the MB-oscillation contribution could be increasing, while differing in phase by more than 90°. The γ_1^1 (40°) and μ_1^6 (40°) decreases presumably are due to the two MB effects, (iii) and (vi), plus possibly the sheath current effect (iv). Finally, the C_1^1 (88°) MR oscillation probably is generated by all three small amplitude MR-oscillation mechanisms, its nearly flat behavior in Fig. 6 presumably resulting from approximate cancellation of the effects (iii)–(vi).

B. As a Function of T

dHvA Plots

The plots in Fig. 8 fit straight lines to within ± 1%, for all six cases. The plot slopes determine the effective mass values presented in Table IV via the relationship $S = -2\pi^2 kc(\hbar e H)^{-1}m^*$, and as discussed in Sec. II, these m^* values were used in the Fig. 8 plots, self-consistently. The uncertainties listed in Table IV arise principally from the ± 1% uncertainty in H, except for the cases λ_1^1 (88°) and μ_1^6 (40°), whose uncertainties were dominated by their larger slope uncertainties, arising from their shorter T ranges. There is excellent agreement with other experimental m^* values, when comparison is possible—cyclotron resonance m^* values were determined at most of the present orientations by Zych and Eck[27] and are included in Table IV (second line).

Magnetoresistance Plots

The MR data vs T are presented (Fig. 9) as percentages by which the MR dropped from its value at 1.37 K. Uncertainties as large as ± 2% were assigned because each series of data points was taken over several days, after which the sample's orientation had shifted enough (0.05°) to have possibly changed the MR at $\theta = 88°$ as much as 2%. The MR behavior in Fig. 9 actually presents an interesting problem for future work. Namely, the MR data (R) in each case fit a T^3 curve,

$$R(T) = R(0\,°K)/(1 + cT^3), \qquad (12)$$

very well (see Fig. 9), with a T^4 behavior being not quite ruled out. If these MR drops vs T are due to increasing phonon scattering in τ^{-1}, via $\rho^{yy} = 1/\sigma^{yy} \propto 1/\tau^{-1}$, then a T^3 law is implied for τ^{-1} in ρ^{yy} ($\tau^{-1} \propto 1 + cT^3$). This would violate Kohler's rule, since the zero-field resistivity $\rho(0)$ is conventionally given by the T^5 law ($\tau^{-1} \propto 1 + cT^5$), while a T^6 law has been observed to be more accurate for many materials.[28] It would be very interesting to determine the actual dependence for pure Mg in the low-temperature range—which is now feasible with the help of picovolt-sensitivity measurement techniques. In any case, a T^3 dependence for $\rho(0)$ seems unlikely and the major question remains: why is the MR temperature dependence so different from that of the simple zero-field resistivity? If phonon scattering were somehow very effective in contributing to $\tau^{-1}(H)$ but not to $\tau^{-1}(H = 0)$, this could explain the discrepancy between these two relaxation rates, as a function of T.

Phonon scattering near MB locations can be intersheet scattering, since the phonon momenta at these temperatures are large enough to span the tiny intersheet interval at such locations. At $H = 0$, a scattering event is effective in contributing to τ^{-1} ($H = 0$) only insofar as it can reverse the carrier's velocity, resulting in a phonon scattering effectiveness which is nearly zero but is growing as T^2 to give the extra T^2 in the conventional T^5

law. In $\sigma^{yy}(H)$, however, the criterion for effec-
tiveness is that the scattering event can reverse
the carrier's coordinate $(k_x - \bar{k}_x)$.[29] Phonon events
across the interval at an MB "hot spot" do not re-
verse the carrier's velocity on the average, any
more than small angle phonon events to the same
sheet do; but they *can* reverse the carriers coor-
dinate $(k_x - \bar{k}_x)$, since the orbit center $(\bar{k}_x, \bar{k}_y)$ is
automatically shifted by such an event. Thus it
appears that the Fig. 9 MR behavior may be under-
stood simply in terms of phonon scattering at the
MB "hot spots." Of course phonon scattering else-
where on the FS would give a T^5 (or T^6) contribu-
tion (e.g., $\tau^{-1} \propto 1 + c_1 T^3 + c_2 T^5$), which would domi-
natein the MR dependence at higher tempera-
tures.

$\Delta_\nu \rho$ Plots

Each plotted point (Fig. 7) represents an aver-
age over the data contained in a fixed field range,
divided by the average at the $T = 1.37$ K point, the
normal point. The ratios obtained were then
plotted on a log scale vs T, in Fig. 7. If there
were no point scatter or uncertainty, the tempera-
ture dependence (if any) of the plots would ideally
display the temperature dependence of C_ν^{ij} in Eq.
(10). There is a large amount of point uncertainty,
however. As is usual for dHvA work, we took data
over a field range spanning 10–20 cycles of oscilla-
tion, which did not allow adequate separation of the
desired frequency from the frequency admixture in
the $\Delta_\nu \rho$ signal. On the basis of the following facts,
it appears that little or none of the observed de-
viation from flat behavior would remain if perfect
frequency discrimination were realized. For γ_1^1
(40°), only 15 cycles of data were taken and used
in Fig. 7, against the known 37 cycles per beat in
Fig. 6, at 1.37 K. But at 1.37 and 2.61 K, 36-
cycle field sweeps were also taken, and when these
data were used, the $+18.7\%$ value plotted in Fig. 7
for 2.61 K was lowered to only $+3.7\%$. For μ_1^5
(70°) the data spanned 18 cycles, compared to a
beat apparent in Fig. 6 of approximately 22 cy-
cles, and the temperature dependence was quite
flat.

In order to parametrize the plotted points in
Fig. 7, we used the standard (weighted) least-
squares procedure to fit the straight lines shown.
The slope values and their standard deviations
were then converted directly to effective masses,
or actually mass differences, exactly as for the
corresponding dHvA plots. These mass differences
then determined the mass ratios presented in Table
IV (last line). The slope of the μ_1^5 (88°) plot in
Fig. 7, for example, converted to $+0.03 m^*(\text{dHvA})$
$\pm 0.02 m^*(\text{dHvA})$, determining the mass ratio
$m^*(\Delta_\nu \rho)/m^*(\text{dHvA}) = 1.03 \pm 0.02$.

V. SUMMARY

The small-amplitude MR oscillations in Mg have
been systematically investigated. The data for six
orbits, as a function of field and temperature, are
presented and analyzed within the useful framework
developed in Sec. II. Within this approach, which
depends upon the simultaneously recorded dHvA
amplitude, any deviation from currently accepted
("normal") SdH theory is displayed as a deviation
from flat behavior in plots such as Fig. 6. Four
of the six orbits observed show large deviations
from the theory, by amounts ranging from 25 to
100% over the field ranges in Fig. 6. The results vs T
may also be interesting, Fig. 7, to whatever extent
they are not simply due to the admixture of unwanted
frequencies. Hopefully Mg's complicated Fermi sur-
face has exposed the fullest possible range of behav-
iors (see Fig. 6), as is desired in an initial experiment.

The probable factors in the abnormal field de-
pendence have been comprehensively considered.
It has been shown that MB causes deviations from
the present SdH theory—which does not include
this factor. In addition, it has been shown that two
new non-SdH mechanisms for small-amplitude
MR oscillation (the $\Delta_\nu \vec{B}$ and MB-oscillation mecha-
nisms) also may contribute to an abnormal behav-
ior. Because Mg is already well understood, we
have been able to identify the mechanisms of MR
oscillation, which probably contributed importantly,
for each of the six orbits. The one orbit which
presumably shows an effectively pure-SdH MR os-
cillation, μ_1^5 (70°), may serve as an example of
our analysis of the field dependence: Only a few
percent deviation from normal $\Delta_\nu \rho$ dependence
would be expected if the 8% deviation from MR
$\propto H^2$ were due to MB effects; this would be con-
sistent with the Fig. 6 data.

This first study of small-amplitude MR oscilla-
tions in metals has also revealed several interest-
ing opportunities for further research other than
the field and temperature dependences above.
Among these are nonlinearity and nonsymmetry
with sample current $(\pm I_s)$, self-field effects, rela-
tively large-amplitude higher harmonics and com-
bination frequencies, and an unwanted zero-current
signal. One would expect to encounter these phe-
nomena as experimental problems in any metal, in
small-amplitude MR oscillation work. And because
high-purity metals are necessary for small-ampli-
tude work, further sheath-current research is
called for, both theoretical and experimental.
Most important, *quantitative* understanding of the
field and temperature dependence of the ordinary
magnetoresistance is needed for *any* material, as
a prerequisite to interpreting of the MR oscillations.

The care which is necessary in interpreting the field
dependence of any given MR oscillation—especially

when the MR field dependence is not yet quantitatively understood—is pointed up by the present results. Despite the variety of dependences in Fig. 6, most of the plots were apparently straight-line fits; these MR oscillations therefore *might* have been thought to obey present SdH theory, within the conventional approach without simultaneously recorded dHvA data.

ACKNOWLEDGMENTS

I am very grateful to Professor R. W. Stark for his help and advice, from suggesting this topic to reading the final manuscript, and for providing the major experimental facilities. This work has also been aided by discussions with S. Auluck, D. R. Baraff, and C. B. Friedberg.

APPENDIX

The effect of intralevel scattering on the transverse elements σ^{ii} ($i = x$ or y) is to introduce the last three terms in Eq. (A1), [13,14]

$$\frac{\sigma^{ii}}{\sigma_0^{ii}} = 1 + \frac{5}{2}\left(\frac{\hbar\omega}{2\zeta}\right)^{1/2} \sum_{r=1}^{\infty} \frac{(-1)^r}{\sqrt{r}}\, e_r \cos\left(2\pi r\,\frac{\zeta}{\hbar\omega} - \frac{\pi}{4}\right) - \frac{3}{4}\frac{\hbar\omega}{2\zeta}\ln(1 - e^{-2X_D})$$

$$+ \frac{3}{2}\frac{\hbar\omega}{2\zeta}\sum_{r=1}^{\infty}(-1)^r A_r e_r \cos\left(2\pi r\frac{\zeta}{\hbar\omega}\right) + \frac{3}{4}\frac{\hbar\omega}{2\zeta}\sum_{r=2}^{\infty}(-1)^r B_r e_r \sin\left(2\pi r\,\frac{\zeta}{\hbar\omega}\right),\quad (A1)$$

where

$$A_r = \sum_{s=1}^{\infty} \frac{(e^{-2X_D})^s}{s^{1/2}(r+s)^{1/2}},$$

$$B_r = \sum_{s=1}^{r-1} \frac{1}{s^{1/2}(r-s)^{1/2}},$$

and e_r is given by Eq. (2). This expression assumes isotropic elastic scattering, on a spherical model Fermi surface with fixed m^*, and is just Eq. (A24) of Ref. 13 except that the spin factor has been added following Roth and Argyres.[14] Although ζ and X_D (i.e., τ_r^{-1}) are oscillatory, for the large n values of the present investigation one finds that they may be treated as constants, to very good accuracy.

The third term adds to the first or σ_0^{ii} term of Eq. (A1), enhancing σ_0^{ii} by the amount

$$-\tfrac{3}{4}(1/2n)\ln(1 - e^{-2X_D}),\qquad (A2)$$

where $\hbar\omega/\zeta$ has been replaced by $1/n$. The upper limit of the enhancement may be calculated as the value of (A2) for the smallest conceivable effective X_D and n on Mg's complicated FS. We estimate the latter values as $X_D = 0.21$ and $n = 75$ [which are the actual values for μ_1^5 (88°) at 36 kG and 1.37 K, from Table I]. The calculation yields (A2)

$= +(\tfrac{1}{200})1.07 = 0.00535$—the enhancement of σ_0^{ii} is $\leq 0.55\%$ at 36 kG and 1.37 K.

Only the fourth term of Eq. (A1) enhances the fundamental oscillation in the second term [which is the $\Delta_\nu \sigma^{ii}/\sigma_0^{ii}$ ratio of Eq. (2)], since the fifth term contains no $r = 1$ contribution. For small enhancements the resulting enhancement value is (A3),

$$\tfrac{1}{2}\tfrac{3}{5}(1/n)^{1/2}A_1,\qquad (A3)$$

where

$$A_1 = \sum_{s=1}^{\infty} \frac{(e^{-2X_D})^s}{s^{1/2}(1+s)^{1/2}}.$$

The calculation of the largest fundamental enhancement, using the smallest values of X_D and n (0.366 and 134) attained in the present experiment—for the case μ_1^5 (88°) at 20.18 kG and 1.35 K—yields the value Eq. (A3) ≤ 0.0127 or 1.27%. But Eq. (A3) overestimates the enhancement at an extremal orbit ν on Mg's actual FS because the fraction of the total density of states in the stationary or central section at ν is actually less that $(1/8n)^{1/2}$, the spherical FS value[30] used in Eq. (A3). Therefore, we conclude that the fundamental enhancement due to isotropic elastic intralevel scattering is $\leq 1\%$ in the present investigation.

[1] F. E. Richards and R. W. Stark, Bull. Am. Phys. Soc. **15**, 91 (1970).

[2] L. M. Falicov, A. B. Pippard, and Paul R. Sievert, Phys. Rev. **151**, 498 (1966).

[3] R. W. Stark and L. M. Falicov, in *Progress in Low Temperature Physics*, edited by C. J. Gorter (North-Holland, Amsterdam, 1967), Vol. V, pp. 235–286.

[4] R. W. Stark and C. B. Friedberg, Phys. Rev. Lett. **26**, 556 (1971), and Proceedings of the Thirteenth International Conference on Low Temperature Physics, 1973 (unpublished).

[5] J. K. Hulbert and R. C. Young, Phys. Rev. Lett. **27**, 1048 (1971).

[6] R. W. Stark and C. B. Friedberg (unpublished).

[7] J. B. Ketterson and R. W. Stark, Phys. Rev. **156**, 748 (1967).

[8] R. W. Stark, Phys. Rev. **162**, 589 (1967).

[9] J. C. Kimball, R. W. Stark, and F. M. Mueller, Phys. Rev. **162**, 600 (1967).

[10]C. B. Friedberg and R. W. Stark, Phys. Rev. B **5**, 2844 (1972).

[11]A. V. Gold, in *Solid States Physics*, edited by J. F. Cochran and R. R. Haering (Gordon and Breach, New York, 1968), Vol. 1, pp. 39–126. Gold's Eq. 28 can be integrated over the Fermi surface ($\epsilon = \zeta$) to give $\mathfrak{N} = \mathfrak{N}_0 + \Sigma_\nu \Delta_\nu \mathfrak{N}$. Also, the spin factor can be added following pp. 60–62.

[12]E. N. Adams and T. D. Holstein, J. Phys. Chem. Solids **10**, 254 (1959).

[13]Ryogo Kubo, Satoru J. Miyaki, and Natsuki Hashitsume, in *Solid State Physics*, edited by Frederick Seitz and David Turnbull (Academic, New York, 1965), Vol. 17, pp. 269–364.

[14]Laura M. Roth and Petros N. Argyres, in *Semi-Conductors and Semi-Metals*, edited by R. K. Willardson and Albert C. Beer (Academic, New York, 1966), Vol. 1, pp. 159–202.

[15]A. B. Pippard, in *Reports on Progress in Physics*, edited by A. C. Strickland (The Physical Society, London, 1960), Vol. XXIII, pp. 176–266; See pp. 213–18.

[16]I. M. Lifshitz, M. Ia Azbel', and M. I. Kaganov, Zh. Eksp. Teor. Fiz. **31**, 63 (1956) [Sov. Phys.-JETP **4**, 41 (1957)].

[17]A. B. Pippard, *The Dynamics of Conduction Electrons* (Gordon and Breach, New York, 1965), pp. 21, 22, and 109.

[18]A. B. Pippard, in Ref. 15, p. 215. Pippard used the notation $(d/dH)\Delta_\nu M$ for $(\partial/\partial H)\Delta_\nu M_z$.

[19]A. B. Pippard, in Ref. 15, p. 217: "Since the oscillations in ρ^{ij} are so intimately related to those of magnetic moment it is not to be expected that the information obtained from each should differ, and the question of which is to be preferred is solely a matter of convenience and ease of observation."

[20]In view of the nonuniformity of any crystal on the microscopic scale, *each* r-space orbit location defines a different state; therefore, even a small angle event scatters the carrier into a new state, at a new r-space location.

[21]R. W. Stark and L. R. Windmiller, Cryogenics **8**, 272 (1968).

[22]F. E. Richards, in Proceedings of the Thirteenth International Confernece on Low Temperature Physics, 1973 (unpublished), and to be published. For degenerate materials and isotropic elastic scattering the general form given, $\sigma^{yy} = c^2\hbar^2H^{-2}\int dN_k(-\partial f_k^0/\partial\epsilon)(k_x - \bar{k}_x)^2 t_k^{-1}$, reduces to the expression in the text. As expressed by Gold (Ref. 23) the appropriate dN_k differential of the number of states per cc is a sum over the differentials dN_α for each orbit α in the dk_z slice, i.e., $dN_k = \Sigma_\alpha dN_\alpha$, where $dN_\alpha = d\epsilon d\mathfrak{N}_\alpha$; and since the well-known factor $-\partial f_k^0/\partial\epsilon$ acts as a δ function at the Fermi energy (Ref. 1) the energy integration thus drops out, leaving the FS integral in the text. The scattering quantity t_k^{-1} is considered in Ref. 24.

[23]A. V. Gold, in Ref. 11, pp. 56–58. Gold used the notation dk_H for dk_z, $\phi_0 dk_H$ for $d\mathfrak{N}_\alpha$ and $\phi_0 dk_H \, d\epsilon$ for the number of states differential $d N_\alpha = d\mathfrak{N}_\alpha d\epsilon$.

[24]For isotropic elastic scattering it is easily confirmed that the general quantity t^{-1}_k given in Ref. 22 reduces to the expression τ^{-1} given in the text, following the notation $[P(\epsilon)$, etc.] and treatment of R. G. Chambers (Ref. 11, p. 314).

[25]See A. B. Pippard, in *the Physics of Metals*, edited by J. M. Ziman (Cambridge U. P., Cambridge, England, 1969), Vol. 1, pp. 113–174, and the references given therein.

[26]R. C. Young, J. Phys. C **4**, 474 (1971), see pp. 489 and 490.

[27]D. A. Zych and T. G. Eck, Phys. Rev. B **1**, 4639 (1970).

[28]See the references given by M. Kaveh and N. Wiser, Phys. Rev. Lett. **26**, 635 (1971).

[29]The scattering event $k \to k'$ contributes to t_k^{-1} (an integral over k', given in Ref. 22) with a relative weight, $1 - (k'_x - \bar{k}'_x)/(k_x - \bar{k}_x)$. In other words, the scattering event is effective according to how much it reverses the carrier's coordinate $k_x - \bar{k}_x$.

[30]A. B. Pippard, in Ref. 17, p. 109.